

1 **Modeling Arctic sea-ice algae: Physical drivers of**
2 **spatial distribution and algae phenology**

3 **Giulia Castellani¹, Martin Losch¹, Benjamin A. Lange^{1,2}, Hauke Flores^{1,2}**

4 ¹Alfred Wegener Institute Helmholtz-Zentrum für Polar- und Meeresforschung, Bremerhaven, Germany.

5 ²University of Hamburg, Zoological Institute and Zoological Museum, Biocenter Grindel, Hamburg,
6 Germany.

7 **Key Points:**

- 8 • Presentation of a new Sea Ice Model for Bottom Algae (SIMBA)
9 • Study of sea-ice algae phenology as function of physical drivers
10 • Assessment of the role of ridged ice as a habitat for sea-ice algae

Corresponding author: Giulia Castellani, giulia.castellani@awi.de

Abstract

Algae growing in sea ice represent a source of carbon for sympagic and pelagic ecosystems, and contribute to the biological carbon pump. The biophysical habitat of sea ice on large scales and the physical drivers of algae phenology are key to understanding Arctic ecosystem dynamics and for predicting its response to ongoing Arctic climate change. In addition, quantifying potential feedback mechanisms between algae and physical processes is particularly important during a time of great change. These mechanisms include a shading effect due to the presence of algae, and increased basal ice melt. The present study shows pan-Arctic results obtained from a new Sea Ice Model for Bottom Algae (SIMBA) coupled with a 3D sea-ice–ocean model. The model is evaluated with data collected during a ship-based campaign to the Eastern Central Arctic in summer 2012. The algal bloom is triggered by light, and shows a latitudinal dependency. Snow and ice also play a key role in ice algal growth. Simulations show that after the spring bloom, algae are nutrient-limited before the end of summer and finally they leave the ice habitat during ice melt. The spatial distribution of ice algae at the end of summer agrees with available observations, and it emphasizes the importance of thicker sea-ice regions for hosting biomass. Particular attention is given to the distinction between level ice and ridged ice. Ridge-associated algae are strongly light-limited, but they can thrive towards the end of summer, and represent an additional carbon source during the transition into polar night.

1 Introduction

Sea ice algae are mainly confined to the network of liquid brine inclusions distributed within the ice matrix. This network forms a protected and stable environment. Sea ice algae are carbon fixers, and constitute an important component of the Arctic marine carbon cycle: almost 60% of primary production in the central Arctic Ocean is attributed to ice algae [Gosselin *et al.*, 1997; Dupont, 2012; Fernández-Méndez *et al.*, 2015, 2016]. Moreover, sea-ice algae can represent the majority of the dietary carbon consumption of key Arctic species such as *Calanus glacialis* [Kohlbach *et al.*, 2016]. Through feeding, carbon produced by sea-ice algae is transferred to higher trophic level species such as polar cod *Boreogadus saida*, thus ice algae represent an essential component for the entire Arctic marine food web [Kohlbach *et al.*, 2016, 2017]. As the phytoplankton and ice algal blooms do not coincide in time or space [Lizotte, 2001], ice algae may extend the growing and primary production period by one to three months [Jin *et al.*, 2012; Tremblay *et al.*, 2008]. Subsequently, the

43 expected changes to timing, magnitude, and spatial distribution of sea ice algal blooms will
44 likely have a direct impact on higher trophic levels [Søreide *et al.*, 2013; Wassmann *et al.*,
45 2006]. In an era characterized by a rapidly changing sea ice cover [Serreze *et al.*, 2003, 2007;
46 Stroeve *et al.*, 2007, 2012a,b; Kwok and Rothrock, 2009; Laxon *et al.*, 2013; Haas *et al.*, 2008;
47 Comiso, 2012; Nicolaus *et al.*, 2012], understanding the temporal and spatial variability of
48 ice associated biomass, and the main physical drivers of algal growth and survival is essential
49 for predicting the fate of sea-ice algae and the consequences on the Arctic marine food web.

50 Ice algal growth is primarily regulated by light [Michel *et al.*, 1988; Welch and Bergmann,
51 1989] and nutrients [Cota *et al.*, 1987]. Light availability is controlled by incoming short-
52 wave radiation, albedo, sea-ice topography and snow, whereas nutrients are supplied to the
53 ice algae through brine drainage, in situ regeneration of biogenic material and exchange
54 with the mixed layer. All these processes are principally regulated by dynamic and ther-
55 modynamic processes within sea ice, and at the atmosphere-ice and ice-ocean interfaces.
56 Consequently, these processes differ among seasons and regions in the Arctic Ocean. In
57 spring, light transmission is mainly regulated by the snow distribution [Perovich, 1996],
58 which in turn is shaped by the surface undulation as consequence of deformation and differ-
59 ential melt processes [Iacozza and Barber, 1999; Lange *et al.*, 2017]. In late spring, higher
60 sea-ice temperatures allow brine drainage due to melting. At the same time, the bottom
61 of the ice becomes permeable and this allows exchange of nutrients with the underlying
62 ocean. In summer, after most of the snow has melted, light transmission depends mainly
63 on ice thickness and surface albedo. Still in summer, when the ocean surface is above freez-
64 ing temperature, basal ice melt represents the largest algal loss [Grossi *et al.*, 1987; Lavoie
65 *et al.*, 2005]. Ice algae phenology is thus affected by different physical processes depending
66 on season and region, and the spatial distribution of algal biomass at the end of summer is
67 a result of the succession and interplay of different physical processes.

68 In situ observations in the Arctic, such as sea-ice cores, are difficult to obtain and
69 hence sparse. Moreover, the spatial distribution of algal chl *a* is driven by the succession
70 of physical events preceding the sampling. Additionally, the physical regimes of the sea ice
71 cover are so heterogeneous that it is hard to assess whether the sparse data are representative
72 of the region sampled. In particular, sea-ice environments such as ridged ice and thick old ice
73 are undersampled, thus our understanding of sea ice algae biogeochemistry is likely biased
74 [Lange *et al.*, 2017]. Recent developments in the retrieval of sea ice algal chl *a* biomass based
75 on under-ice hyperspectral measurements acquired from under-ice profiling platforms, such

76 as Remotely Operated Vehicles (ROV) and the Surface and Under Ice Trawl (SUIT), enabled
77 the retrieval of ice algal chl *a* biomass on scales of meters to kilometers [*Melbourne-Thomas*
78 *et al.*, 2015, 2016; *Lange et al.*, 2016; *Meiners et al.*, 2017]. Advancements in satellite-based
79 remote sensing during the past decades have vastly improved the monitoring of sea-ice extent
80 [*Stroeve et al.*, 2012b; *Ivanova et al.*, 2014], thickness [*Kwok et al.*, 2009; *Laxon et al.*, 2013;
81 *Ricker et al.*, 2015; *Tilling et al.*, 2015], ocean surface chl *a* concentration and derived NPP
82 [*Arrigo and van Dijken*, 2011]. Still, ice associated algae and phytoplankton in ice covered
83 regions cannot be observed by satellite, so that a comprehensive picture of their distribution
84 on large scales remains difficult to obtain.

85 Numerical models can serve as tools to fill the gaps incurred by the methodological
86 difficulties in observing the ice environment. Models can also be used to simulate bio-
87 geochemical processes and ice algal dynamics on regional to basin scales, along with their
88 seasonal evolution, and help identify the main physical processes affecting sea-ice algae phe-
89 nology. Moreover, they are ideal tools for studying possible feedback mechanisms between
90 biological processes and the physical system.

91 Early sea-ice biogeochemical models were mainly focused on Antarctic sea ice [e.g.
92 *Arrigo et al.*, 1993, 1997], and provided the foundation for understanding and modeling
93 mechanisms that drive the seasonality of ecosystems in sea ice [*Arrigo et al.*, 1993] and
94 the large scale algal biomass distribution for the entire sea-ice pack [*Arrigo et al.*, 1997].
95 Modeling efforts since then mainly fall into two categories [*Vancoppenolle and Tedesco*, 2017]:
96 (1) understanding and testing drivers of ecosystems in sea ice [*Arrigo et al.*, 1993; *Lavoie*
97 *et al.*, 2005; *Jin et al.*, 2006; *Tedesco et al.*, 2010; *Saenz and Arrigo*, 2014; *Belém*, 2002;
98 *Mortensen et al.*, 2017]; (2) quantifying large scale quantities, in particular, total biomass
99 and primary production [*Sibert et al.*, 2010; *Deal et al.*, 2011; *Jin et al.*, 2012; *Dupont*, 2012].

100 In this study, we introduce a simple biogeochemical model for algal growth in a coupled
101 3D sea-ice–ocean model of the Arctic Ocean circulation. A model run for one year is used to
102 identify the main physical drivers of sea-ice algal growth and decay. The spatial variability
103 of algal chl *a* in late summer is related to the spatial variability of physical sea-ice parameters
104 in the Arctic Ocean. The novelty of this work is the study of sea-ice algae associated to
105 different sea-ice classes. Particular attention is given to ridged and deformed ice, which is
106 difficult to sample and, as a consequence, commonly overlooked as potential algal growth
107 sites [*Kuparinen et al.*, 2007; *Meiners et al.*, 2012; *Vancoppenolle et al.*, 2013; *Lange et al.*,

2015]. Finally, possible feedbacks between the ocean–sea-ice system and sea-ice algae are investigated. Our simulations focus on 2012, in order to compare results with observations acquired during late summer of the same year [Lange *et al.*, 2016, Lange *et al.*, *Spatial variability of summertime Arctic sea-ice algae biomass and primary production estimates* (Under Revision), later referred to as BLROV].

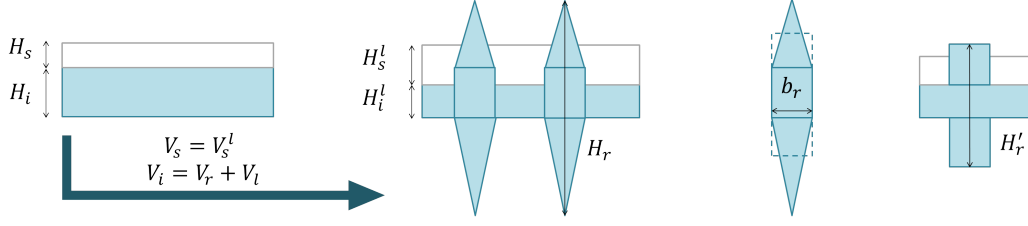
2 Model description

2.1 Dynamic sea-ice–ocean model

We use the Massachusetts Institute of Technology general circulation model (MITgcm) in a coupled ocean–sea-ice Arctic Ocean configuration [Marshall *et al.*, 1997; Castro-Morales *et al.*, 2014]. The domain covers the Arctic Ocean, the Nordic Seas, and the North Atlantic with a southern limit of approximately 50°N. The horizontal resolution of 1/4° corresponds to a grid spacing of ~ 28 km on a rotated spherical grid with the grid equator passing through the geographical North Pole. The ocean is discretized into 33 vertical layers ranging from ~ 10 m at the surface to ~ 350 m at maximum depth. The ocean model is coupled with a dynamic-thermodynamic sea-ice model [Losch *et al.*, 2010]. The sea-ice model uses a viscous-plastic rheology and the so-called zero-layer thermodynamics (i.e., zero heat capacity formulation) [Semtner, 1976] with a prescribed ice thickness distribution [Hibler, 1979, 1980, 1984; Castro-Morales *et al.*, 2014]. The model is forced by atmospheric fields of the NCEP Climate Forecast System Version 2 (CFSv2) for 2012 [Saha *et al.*, 2014]. The data set includes fields for 6-hourly wind at 10 m, atmospheric temperature and specific humidity at 2 m, daily downward long and short-radiative fluxes, and a monthly precipitation field. A monthly climatology of river runoff for the main Arctic rivers follows the Arctic Ocean Model Intercomparison Project protocol [AOMIP, Proshutinsky *et al.*, 2001]. The coupled sea-ice–ocean model is spun-up from 1948 to 1978 with the Coordinated Ocean Research Experiment (CORE) Version 2 data and then with the NCEP (CFSv2) from 1979 to the end of 2011.

2.1.1 Ice and snow volume redistribution due to ridges

In our configuration, the sea-ice model does not contain a dynamic thickness redistribution function. This means that for each grid cell we know only the mean thickness and there is no explicit information about ridges. In order to differentiate between level ice and



144 **Figure 1.** Scheme of grid-averaged sea-ice volume (V_i) and snow volume (V_s) redistribution into
 145 level ice volume and level snow volume (V_l and V_s^l) and ridged ice volume (V_r). The notation refers
 146 to: grid-averaged sea-ice thickness (also called parental ice) H_i ; Snow thickness on grid-averaged
 147 sea ice H_s ; Level sea-ice thickness H_i^l and snow thickness on level ice H_s^l ; Total thickness H_r and
 148 base b_r of ridges; Final thickness of ridges $H_r' = 2.91 \text{ m} + H_i$ (see also Section 2.1.1).

138 ridged ice, we use the energy that accumulates in sea ice due to deformation [*Steiner et al.*,
 139 1999; *Castellani*, 2014]. The deformation energy R is the result of internal sea-ice stresses;
 140 it is used to estimate the ridge density S_d based on geometrical constraints [*Steiner et al.*,
 141 1999] and ice thickness H_i . We use a modified equation from *Steiner et al.* [1999] that avoids
 142 unrealistically large numbers of ridges for thickness values lower than 1:

$$143 \quad S_d = \frac{R}{c_n} \cdot \begin{cases} e^{-\frac{(H_i-1)^2}{0.2}} & \text{for } H_i \leq 1 \\ e^{-\frac{(H_i-1)^2}{3}} & \text{for } H_i > 1 \end{cases} . \quad (1)$$

154 Table 1 summarizes the parameter values. In order to estimate the ice thickness for
 155 level and ridged ice in each grid cell, the following assumptions are made: 1) A ridge is
 156 formed by two triangles (sail and keel) sharing the same base. The base is considered to
 157 be a rectangle as thick as the parental ice, referred to as grid-averaged sea ice, H_i (Figure
 158 1). 2) The ratio between vertical keel and sail cross section areas is set to 3.85 [*Timco and*
 159 *Burden*, 1997]. 3) The height of the sail above level ice is estimated to be the same for all
 160 ridges with a value of $H_{\text{sail}} = 1.2 \text{ m}$ [*Castellani et al.*, 2014] and the slope angle of the sides
 161 is taken as $\beta = 23^\circ$ [*Steiner et al.*, 1999], which gives a ridge base of $b_r = 5.65 \text{ m}$. The
 162 edges of the ridges transmit more light than the central part, where the maximum thickness
 163 is found. In order to account for these differences, we redistribute the area of the ridges
 164 into a rectangle, and thus we compute an equivalent thickness of $H_r' = 2.91 \text{ m} + H_i$, where
 165 H_i is the thickness of the parental ice (grid-averaged sea ice) and the value 2.91 m is the
 166 result of the redistribution of the sail and keel cross section areas into a rectangle. Thus, the

149 **Table 1.** List of variables and parameters, and corresponding description and units used in the
 150 model. Variables are marked as computed by the model or read as external field. Parameters
 151 superscript refers to the source: a) *Lavoie et al.* [2005], b) *Grenfell and Maykut* [1977], c) *Steiner*
 152 *et al.* [1999], d) *Zeebe et al.* [1996], e) *Sarthou et al.* [2005], f) *Perovich* [1996], g) tuned with 1D
 153 experiments, h) *Vancoppenolle and Tedesco* [2017], i) as in the MITgcm.

Variable	Definition	Computed/read	Unit
B	Ice algal biomass concentration	computed	mg chl a m^{-3}
D	Detritus concentration	computed	mg m^{-3}
F_{ia}	Energy released as heat by sea-ice algae	computed	W m^{-2}
H_i	Ice thickness	computed	m
H_s	Snow thickness	computed	m
H_i^l	Thickness of level ice	computed	m
H_s^l	Thickness of snow on level ice	computed	m
H_r^l	Thickness of ridged ice	computed	m
I_0	Shortwave incoming radiation	external field	W m^{-2}
k_B	Algae attenuation coefficient	computed	m^{-1}
\tilde{M}	Melt rate at the bottom of sea ice	computed	$m s^{-1}$
\tilde{M}_B	Bottom melt caused by heat released by algae	computed	$m s^{-1}$
μ	Growth rate	computed	d^{-1}
N	Nitrate concentration	computed	mg m^{-3}
PAR	Photosynthetic active radiation	computed	$\mu\text{Einst } m^{-2} s^{-1}$
R	Deformation energy	computed	J m^{-2}
S_d	Ridge density	computed	nr m^{-1}
Parameter	Definition	Value	Unit
α	Albedo	see Table 2	dimensionless
a^*	Mean chl a specific attenuation coefficient ^{a)}	0.02	$m^2 (\text{mg chl } a)^{-1}$
α_B	Photosynthetic efficiency ^{a)}	0.07	mg C (mg chl a) ⁻¹ h ⁻¹ ($\mu\text{Einst } m^{-2} s^{-1}$) ⁻¹
b_r	Base length of ridges	5.65	m
C_0	Surface transmission parameter ^{b)}	0.3	dimensionless
c_n	Proportionality constant for ridge density calculation ^{c)}	$14 \cdot 10^3$	$J^{1/2} m^{-1/2}$
δz	Bottom layer occupied by sea ice algae ^{a)}	0.05	m
F_r	Fraction of absorbed energy released as heat by algae ^{d)}	0.9	dimensionless
k_N	Half saturation constant for nitrate uptake ^{c)}	0.1	mg m^{-3}
k_i	Ice attenuation coefficient ^{a,f)}	1.5	m^{-1}
k_s	Snow attenuation coefficient ^{f)}	5	m^{-1}
L_i	Latent heat of fusion of sea ice ^{d)}	283	KJ kg^{-1}
λ_{mo}	Mortality rate ^{g)}	0.02	d^{-1}
$\lambda_{up/re}$	Uptake and respiration rate ^{g)}	0.01	d^{-1}
λ_{rm}	Remineralization rate ^{g)}	0.01	d^{-1}
μ_M	Maximum ice algal specific growth rate ^{h)}	0.86	d^{-1}
P_m	Maximum photosynthetic rate ^{a)}	0.28	mg C (mg chl a) ⁻¹ h ⁻¹
ρ_i	Sea ice density ⁱ⁾	910	kg m^{-3}

167 thickness of the ridged ice is different for each grid cell due to changes in the grid-averaged
 168 sea-ice thickness H_i . The ridges are assumed to be parallel to one of the grid sides, and
 169 to extend over the whole length of the grid cell. The ice volume is then redistributed into
 170 ridged ice and level ice, giving a thickness of level ice:

$$171 \quad H_i^l = \frac{H_i - H_r' b_r S_d}{1 - S_d b_r}. \quad (2)$$

172 All parameters and variables in equation 2 and equation 3 are listed in Table 1. Ridges are
 173 assumed to be practically snow free [*Iacoza and Barber, 1999; Sturm et al., 2002; Perovich*
 174 *et al., 2003*], so that the snow on level ice has the thickness:

$$175 \quad H_s^l = \frac{H_s}{1 - S_d b_r}. \quad (3)$$

176 The distinction between level ice and ridged ice and, as explained in Section 2.1.2, their
 177 effect on light transmission is used only to drive the algal model (and for diagnostics), but
 178 does not affect the thermodynamic and dynamic processes of the model.

179 **2.1.2 Light attenuation through snow and ice**

180 In the MITgcm, the heat fluxes through ice are computed following *Hibler* [1984].
 181 The mean ice thickness (i.e., the grid-averaged sea-ice thickness) is distributed into seven
 182 ice thickness categories between 0 and a maximum thickness of twice the mean thickness.
 183 The distribution of these seven thicknesses is flat, normalized and fixed in time (see *Hibler*
 184 [1984] and *Castro-Morales et al.* [2014], their Figure 1). The snow follows the same thickness
 185 distribution so that thin ice is covered by a thin snow layer and thick ice by a thick snow layer
 186 [*Castro-Morales et al., 2014*]. The heat flux is computed for each thickness category. Then all
 187 the heat fluxes are averaged to give the net heat flux that is responsible for thermodynamic
 188 processes such as basal melting or freezing. Note that in this sub-grid parameterization,
 189 some part of the grid always contains thin ice of $\frac{1}{7}$ of the mean thickness, which allows
 190 a finite heat flux even for thick mean ice. The light transmission through each thickness
 191 category follows the Beer-Lamber law:

$$192 \quad I^{(c)}(H_i^{(c)}, H_s^{(c)}) = I_0(1 - \alpha)C_0 e^{-k_i H_i^{(c)} - k_s H_s^{(c)}}, \quad (4)$$

193 where $H_i^{(c)}$ and $H_s^{(c)}$ are the ice thickness and snow thickness of category c , I_0 the incoming
 194 shortwave radiation, and α the albedo. The albedo depends on snow and ice types, as listed
 195 in Table 2. The surface transmission parameter $C_0 = 0.3$ accounts for that part of incoming
 196 radiation absorbed in the first few centimeters of the ice [*Grenfell and Maykut, 1977*]. k_i

212 **Table 2.** Values for albedo as a function of surface (ice and snow) conditions used in the sea-ice
 213 package of the MITgcm.

Surface Conditions	Albedo α
Dry ice	0.70
Wet ice	0.68
Dry snow	0.81
Wet snow	0.77

197 and k_s are constant attenuation coefficients for sea ice and snow [Lavoie *et al.*, 2005]. For
 198 a detailed review of ice and snow attenuation coefficients see Perovich [1996]. In our study,
 199 the algae are assumed to occupy only a bottom layer of 5 cm of the sea ice [Vancoppenolle
 200 and Tedesco, 2017; Lavoie *et al.*, 2005; Jin *et al.*, 2006; Dupont, 2012] (see Section 2.2) so
 201 that there is no self-shading effect due to ice algae above the bottom layer.

202 The light transmission through grid-averaged sea ice is computed according to equation 4
 203 with the same values of k_i and k_s (Table 1) for each thickness category. The transmitted
 204 shortwave radiation (light) fluxes are summed to give the net shortwave heat flux that
 205 penetrates into the ocean. In the case of the redistributed ice into level and ridged ice
 206 (Section 2.1.1), the light transmission through level ice, excluding the ridges, is computed
 207 in accordance to the grid averaged ice with the same attenuation parameters and using the
 208 same thickness distribution. Ridged ice is assumed to occupy only one separate category
 209 for which we assume a smaller $k_i = 0.8 \text{ m}^{-1}$ due to the higher porosity of ridges. To avoid
 210 any confounding effects, the ocean is not affected by the modified light transmission based
 211 on the redistribution into level ice and ridged ice.

214 **2.2 SIMBA: Sea Ice Model for Bottom Algae**

215 The new Sea Ice Model for Bottom Algae (SIMBA) has one class of algae, one for
 216 nutrients and one for detritus. Nitrate represents the nutrients because it is typically con-
 217 sidered the limiting nutrient for ice algal growth in fully marine waters [Smith *et al.*, 1997].
 218 We assume that the ice algae occupy a bottom layer of thickness δz of 5 cm [see also Lavoie
 219 *et al.*, 2005; Jin *et al.*, 2006; Dupont, 2012; Lange *et al.*, 2015]. We consider four main biolog-
 220 ical processes responsible for changes in algae, nutrient and detritus concentrations: uptake

221 of nutrients from the algae, respiration transforming algae back into nutrients, mortality
 222 of algae that are then transformed into detritus, and remineralization, which describes the
 223 decomposition of organic matter, i.e., detritus converted back into nutrients. The physical
 224 processes affecting algae, nutrient and detritus are light limitation, sea-ice basal melting
 225 (melting of ice results in removal of ice algae), and horizontal transport of ice (algae are
 226 advected as tracers in sea ice). A term for the resupply of nutrients from the underlying
 227 ocean water is not considered in the present configuration. The equations solved by the
 228 model for ice algae biomass B , nutrient N and detritus D are:

$$229 \quad \frac{dN}{dt} = -(\mu - \lambda_{up/re})B + \lambda_{rm}D \quad (5)$$

$$230 \quad \frac{dB}{dt} = (\mu - \lambda_{up/re})B - \lambda_{mo}B + \frac{\tilde{M}}{\delta z}B \quad (6)$$

$$231 \quad \frac{dD}{dt} = \lambda_{mo}B - \lambda_{rm}D. \quad (7)$$

232 A term for algal loss due to melting is considered in equation (6) where \tilde{M} is the basal melt
 233 rate (m s^{-1}). Melt loss of algae is the only flux of material to the underlying ocean waters.
 234 Parameters describing respiration ($\lambda_{up/re}$), mortality (λ_{mo}) and remineralization (λ_{rm}) are
 235 assumed to be constant (see Table 1).

236 The growth rate μ is a function of nutrient availability $f(N)$ and light availability
 237 $f(PAR)$:

$$238 \quad \mu = \mu_M f(N) f(PAR). \quad (8)$$

239 The term μ_M is a constant and represents the maximum growth rate (see Table 1). The
 240 limitation of photosynthesis by nutrient supply is assumed to follow a Michaelis-Menten
 241 form [*Monod*, 1949]:

$$242 \quad f(N) = \frac{N}{N + k_N}, \quad (9)$$

243 where $k_N = 0.1 \text{ mg m}^{-3}$ is the half saturation constant for nitrate [*Sarthou et al.*, 2005].

244 The response of photosynthesis to light follows *Webb et al.* [1974]:

$$245 \quad f(PAR) = 1 - e^{-\frac{\alpha_B PAR}{P_m}}, \quad (10)$$

246 where PAR (Photosynthetically Active Radiation) is that part of the light spectrum used
 247 for photosynthesis, α_B is the photosynthetic efficiency and P_m is the light saturated specific
 248 photosynthetic rate (or maximum photosynthetic rate). Values for α_B and P_m (Table 1) are
 249 taken as averages of the values suggested in *Lavoie et al.* [2005], their Table 2. To convert
 250 light I from W m^{-2} into PAR in $\mu\text{Einst m}^{-2} \text{ s}^{-1}$ we follow *Vancoppenolle et al.* [2011] and

251 *Lavoie et al.* [2005]:

$$252 \quad PAR = 0.45 \cdot 4.91 \cdot I, \quad (11)$$

253 where 4.91 is the quanta-energetic ratio and 0.45 is the ratio between total number of
 254 incoming quanta in the visible region (0.4 - 0.7 μm) with respect to the number for the
 255 entire shortwave (0.3 - 3 μm) band [*Frouin and Pinker*, 1995].

256 The response of the algal model to the physical forcings provided by the sea-ice-ocean
 257 system for 2012 was tested with 1D experiments (not shown). SIMBA is then applied to
 258 the entire Arctic basin in two different study cases: 1) the case of grid-averaged sea-ice
 259 thickness (Section 3.1), used also to investigate the effects of algae on the sea-ice-ocean
 260 system (Section 3.2); and 2) the case of distinction between level ice and ridged ice (Section
 261 3.3).

262 **2.3 Effects on ice and ocean systems**

263 Since light is also needed for phytoplankton growth under sea ice, the presence of
 264 algae at the bottom might inhibit or delay the under-ice phytoplankton bloom in the surface
 265 ocean. In order to test such an effect, we estimate the light that reaches the ocean surface
 266 following *Lavoie et al.* [2005] and previously *Kirk* [1983] as a function of sea-ice algae chl *a*
 267 concentration. The attenuation coefficient due to algae k_B is

$$268 \quad k_B = a^* \cdot B \quad (12)$$

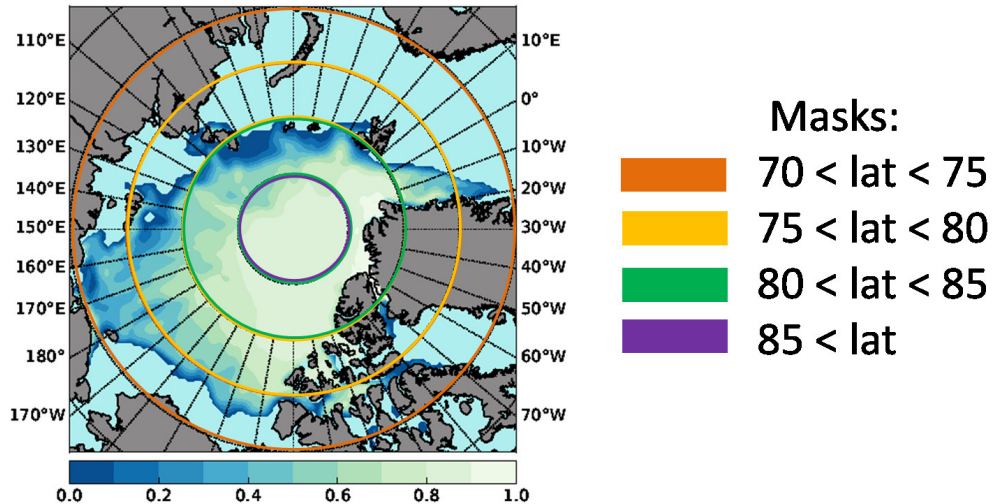
269 with $a^* = 0.02 \text{ m}^2 (\text{mg chl } a)^{-1}$. Adding this term into equation 4 we get:

$$270 \quad I(H_i, H_a, \text{chl } a) = I_0 (1 - \alpha) C_0 e^{-k_i H_i - k_s H_s - k_B \delta z}. \quad (13)$$

271 Ice algae absorb more PAR than that required for photosynthesis. The extra energy is
 272 released as heat, thus contributing to basal ice melt. To quantify such algae-induced melt,
 273 we follow *Lavoie et al.* [2005]:

$$274 \quad \tilde{M}_B = \frac{I(H_i, H_s) F_r (1 - e^{-k_B \delta z})}{\rho_i L_i}, \quad (14)$$

275 where F_r is the fraction of the energy absorbed by the ice algal layer that is released as heat,
 276 L_i is the latent heat for sea ice and ρ_i the density of sea ice. Values for F_r and L_i are taken
 277 from *Zeebe et al.* [1996] and listed in Table 1. These effects are diagnosed and discussed in
 278 Section 3.2, but in our first version of SIMBA they do not feed back into SIMBA nor the
 279 ocean and sea-ice physics.



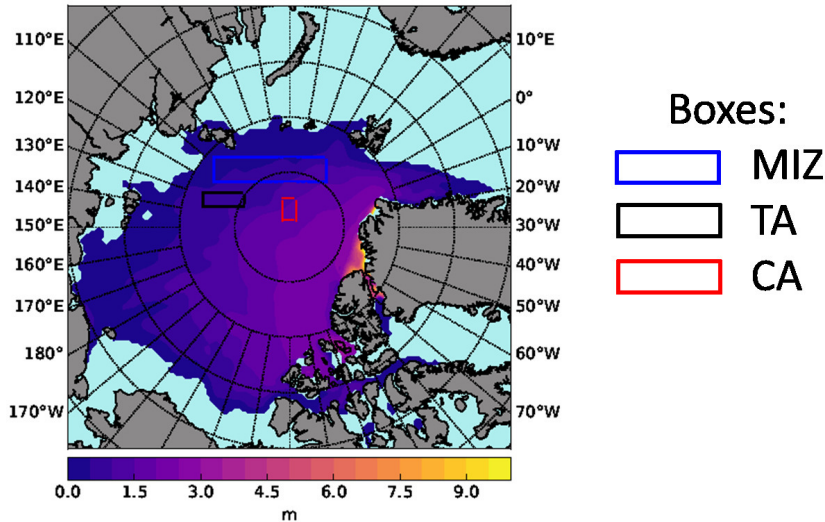
288 **Figure 2.** Map of the model domain with white-blue shades corresponding to the simulated
 289 sea ice concentration in September 2012. The colored rings represent the masking applied to the
 290 domain according to latitude, as explained in Section 3.

280 3 Results

281 3.1 SIMBA applied to grid-averaged sea ice

282 In Figures 2 and 3 we show the simulated sea-ice concentration and the sea-ice thickness
 283 for September 2012, respectively. Areas of interest for our study are also highlighted. We
 284 run the coupled algae–sea-ice–ocean model in a 3D configuration accounting for 5 different
 285 scenarios R0, R2, R4, R6 and R8 representing 5 different initial conditions (see Table 3).
 286 This first comparison allows us to identify the run which has the best agreement with
 287 observations, but also to test the sensitivity to different initial conditions.

300 For a quantitative comparison, we use sea-ice algal chl *a* estimates by BLROV (Table
 301 4). We limit our comparison to the median values shown in Table 1 of BLROV to have
 302 the most representative measurements for comparison with model output on a grid of $1/4^\circ$.
 303 There are two reasons why we focus our comparison mainly on BLROV data. First, the
 304 data were collected in 2012 and allow a direct comparison in time and space. Second the
 305 chl *a* estimates are based on under-ice hyperspectral radiation measurements [*Lange et al.*,
 306 2016] conducted with a ROV over a scale of hundreds of meters, so that they are not
 307 point-measurements and relate better to the grid-cell averages (~ 25 km) of the model. A
 308 qualitative comparison with empirical data is discussed in Section 4.



291 **Figure 3.** Map of the model domain with grid-averaged sea ice thickness for September 2012
 292 depicted by colors. The square boxes represent the areas considered for a comparison with obser-
 293 vations (Section 3): Marginal Ice Zone (MIZ), Transitional Area (TA), and Compact Area (CA).

309 The chl *a* estimates from BLROV are binned in three areas of interest (Figure 3), namely
 310 Marginal Ice Zone (MIZ), Transitional Area (TA) and Compact Area (CA). The averaged
 311 data and the corresponding model values in the same three regions for the 5 different initial
 312 conditions are listed in Table 3. Amongst the 5 runs, R4 shows the best agreement to
 313 observations, thus hereafter our analysis will be restricted to the R4 run, except when
 314 stated otherwise.

319 In September, simulated and observed algae concentrations appear to be low in the
 320 Marginal Ice Zone (Figure 4). The modeled concentrations increase approximately with
 321 latitude and reach a maximum in the Lincoln Sea with values exceeding $10 \text{ mg chl } a \text{ m}^{-2}$.
 322 North of 85°N the algae concentration increases from the eastern sector to the western sector
 323 from $1.29 \text{ mg chl } a \text{ m}^{-2}$ to $4.33 \text{ mg chl } a \text{ m}^{-2}$. The observed mean value for that region is
 324 higher (Table 3) with $4 \text{ mg chl } a \text{ m}^{-2}$ compared to a mean modeled value of $2.81 \text{ mg chl } a$
 325 m^{-2} , but still in the range of variability.

326 In summer (between April and September), more than 1 m of ice melts in the MIZ (Figure
 327 5), but melt rates are low in multi-year ice regions along the coast of Greenland and north
 328 of the Canadian Arctic Archipelago (CAA). In particular, the total melt in the Lincoln sea
 329 is one order of magnitude smaller than in the marginal sea-ice zone.

294 **Table 3.** Initial conditions (mg m^{-2}) for sea-ice algae (B), Nutrient (N) and Detritus (D) in 5
 295 different scenarios (R0, R2, R4, R6 and R8), and mean values of algal chl *a* concentrations (mg
 296 m^{-2}) to be compared with observations in three different regions (see also Fig. 3): Marginal Ice
 297 Zone (MIZ), Transitional Area (TA) and Compact Area (CA). The chl *a* values are averages for
 298 September to be compared with observations. The last row contains the median values from Table
 299 4 to allow an easier comparison with modeled values.

run	Initial conditions (mg m^{-2})			Model predicted mean chl <i>a</i> per region (mg m^{-2})		
	B	N	D	MIZ	TA	CA
R0	50	0.74	0	0.61	0.82	1.32
R2	0.05	50	0	0.76	0.98	1.33
R4	0.05	50	25	1.24	1.57	2.14
R6	0.05	25	25	0.87	1.09	1.51
R8	0.05	0.74	50	0.98	1.21	1.69
Obs	-	-	-	1.23	1.94	4

335 In Figure 6 we show the spring to autumn evolution of under-ice light, sea-ice algal
 336 biomass, nutrients and detritus for four different latitudinal regions between 70° to 75°N ,
 337 75° to 80°N , 80° to 85°N , and greater than 85°N (Figure 2). Table 5 lists key numbers that
 338 characterize the experiments: 1) bloom onset defined as the day when the algae start to
 339 grow exponentially, inferred from the slope of the curves in Figure 6b; this corresponds to
 340 2) a threshold for PAR to trigger the bloom, i.e. above such value an algal bloom develops;
 341 3) the day when the peak of biomass is reached, identified as the maximum of the curve
 342 (Figure 6b); 4) the maximum biomass value. We note, that the threshold value for PAR
 343 should not be confused with the threshold for algal growth, since the algae start growing
 344 already at lower values.

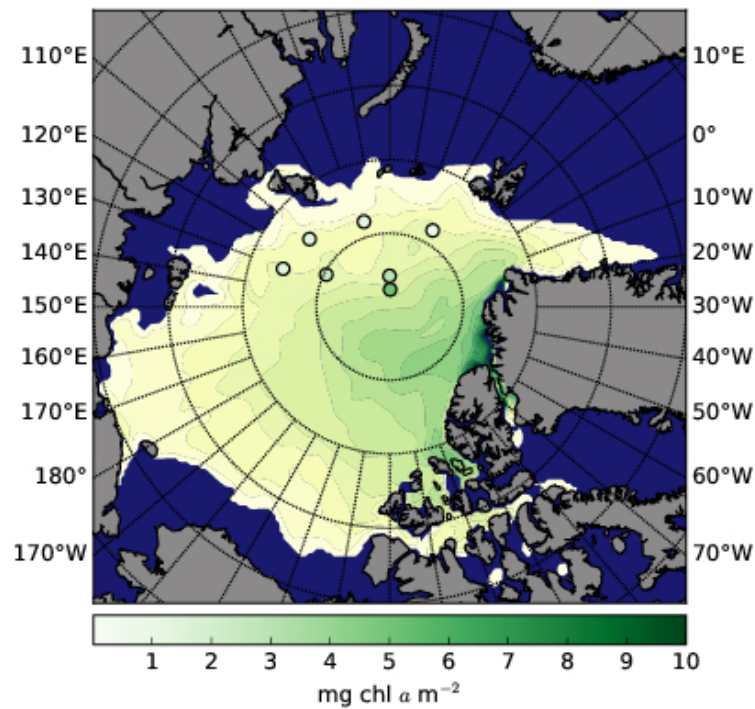
350 Onset of algal bloom and time of maximum biomass differ from region to region (Figure
 351 6 and Table 5). South of 75°N , the growth becomes exponential already at the end of March
 352 (day 87), followed by more northern regions. For the area north of 85°N bloom onset is 40

315 **Table 4.** Sea-ice algal chl a (mg m^{-2}) from BLROV. Measurements were undertaken at the end of
 316 August and in September 2012, the locations are shown in Figure 4. Values are averaged according
 317 to region (see also Figure 3) and refer to median, 75% of median (assuming that 75% of the total
 318 biomass lies in the bottom part), 25th percentile (IQR25) and 75th percentile (IQR75).

study area	mg chl a m^{-2}			
	median	75% median	IQR25	IQR75
MIZ	1.23	0.86	1.15	1.36
TA	1.94	1.46	1.66	2.32
CA	4	3	2.15	6.7

353 days later than in the southernmost region. A similar delay is seen in the timing of maximum
 354 biomass with a gap of 30 days between the southernmost sector and the northernmost sector.
 355 Note, that the bloom in the region north of 85°N develops faster, reaching its maximum in
 356 21 days compared to ~ 33 days for the other regions. North of 85°N the maximum algal
 357 biomass is also larger, with $50 \text{ mg chl } a \text{ m}^{-2}$ compared to the mean of $\sim 36 \text{ mg chl } a \text{ m}^{-2}$
 358 in other regions. After the peak, algae start dying and reach a minimum at the end of
 359 August. There is also a secondary growth period between September and October, before
 360 algal biomass decreases to its minimum (Figure 6b). This feature has also been reported
 361 in other models [*Jin et al.*, 2006; *Deal et al.*, 2011; *Jin et al.*, 2012; *Ji et al.*, 2013] and
 362 attributed to the detritus compartment. Before the spring bloom, nutrient concentrations
 363 increase slightly (Figure 6c) as inorganic matter remineralizes. When the bloom initiates,
 364 algae consume nutrients until they become nutrient limited. The detritus increases when
 365 algae die.

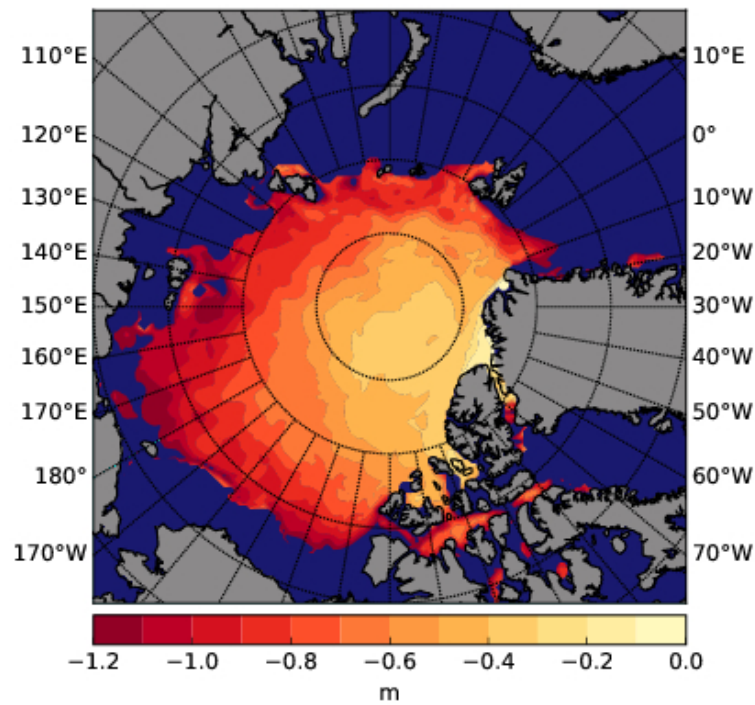
372 The day of bloom onset depends on light availability and therefore on latitude (Figure
 373 7a), but light availability is also affected by other factors. The spatial pattern of these
 374 factors, i.e. snow thickness, ice thickness and snow melt, are remarkably similar to the
 375 bloom onset pattern (Figure 7b-d). From Figure 7a we see an increasing trend from the
 376 Bering Strait to the region north of 85°N , with day of bloom onset going from 90 to 135.
 377 The areas that do not follow this latitudinal dependence are the Kara Sea, Fram Strait and
 378 Lincoln Sea. The day of complete snow melt (Figure 7b) shows values around 130 in the
 379 Beaufort Sea and East Siberian Sea, whereas values are up to 180 for latitudes larger than



330 **Figure 4.** Pan Arctic map of sea-ice algal chl *a* concentration per grid cell simulated for Septem-
 331 ber 2012. The circles represent the ROV based observations from BLROV (see Section 3). Both
 332 observed and simulated values use the same color scale.

380 85°N and in the Nansen Basin. Ice thickness (Figure 7c) is in the range 0.5-3.5 m in most
 381 of the Arctic Ocean, hence in agreement with observations [Ricker *et al.*, 2017], except for
 382 the Lincoln Sea, where thicknesses of up to 10 m represent an overestimation compared to
 383 recent satellite data [Ricker *et al.*, 2017]. Snow thickness ranges between 10 to 40 cm in
 384 the Beaufort Sea, East Siberian Sea, and Laptev Sea, whereas values are up to 1 m in the
 385 Nansen Basin and Kara Sea close to Severnaya Zemlya islands.

389 Monthly values of net primary production NPP are shown in Figure 8. NPP has a
 390 maximum value around 15 mg C m⁻² d⁻¹. The spatial patterns between April and July
 391 resemble the latitudinal dependency of the algal bloom. In April and May values are higher
 392 at the marginal areas than in the central Arctic, whereas the situation is reversed in June
 393 and July. The end of July sees the termination of the major production season in sea ice.



333 **Figure 5.** Total summer basal ice melt (m) integrated over the period April to September 2012
 334 obtained from the sea-ice model.

396 3.2 Estimating effects on ice and ocean physics

397 Algae at the bottom of sea ice absorb light and hence reduce light penetration through
 398 the ice into the ocean surface. In the two latitudinal bands between 70°N, 75°N and 80°N
 399 the light reaching the surface ocean (Figure 9a) remains very close to the mean threshold
 400 value (gray line in Figure 9a) inferred from the light regime without the shading effect
 401 (Figure 6a). In the latitudinal bands north of 80°N the light remains under the threshold
 402 value until mid June. The shading effect is nearly zero before April and then increases to
 403 values up to $2 \mu\text{Einst m}^{-2} \text{s}^{-1}$, or 20 to 30% of the transmitted radiation, in June and July
 404 (Figure 9b).

410 Integrated summer (April to September) algae-induced melt (equation 14) varies be-
 411 tween a minimum of 0.1 cm in the northern regions (particularly north of 85°N and in the
 412 Nansen Basin) and a maximum of 1.5 cm ice loss in the marginal areas (Figure 10). Partic-
 413 ularly high values are found in the East Siberian Sea, north of the Laptev Sea and in the

366 **Table 5.** Key numbers to characterize and compare the numerical experiments: day of bloom
 367 onset defined as the day from beginning of January when the algae start growing exponentially,
 368 inferred from the slope of the curves in Figure 6b; corresponding value of PAR considered as the
 369 threshold for algal bloom; day when the peak of biomass is reached; and value of maximum biomass.
 370 Values are computed for the grid-averaged ice (G-Ave), for level ice (Lev) and for ridged ice (Rid).
 371 Results are divided in four different sectors according to latitude (see also Fig. 2).

ice type	sector	bloom onset (day)	light ($\mu\text{Einst m}^{-2} \text{ s}^{-1}$)	day of max biomass (day)	maximum biomass (mg chl <i>a</i> m^{-2})
G-Ave	70°N < lat < 75°N	87	2	118	37
	75°N < lat < 80°N	95	1.84	132	34
	80°N < lat < 85°N	114	1.65	146	38
	85°N < lat	127	1.49	148	50
Lev	70°N < lat < 75°N	92	1.79	128	37
	75°N < lat < 80°N	102	1.78	139	33
	80°N < lat < 85°N	121	1.40	154	34
	85°N < lat	134	1.56	157	48
Rid	70°N < lat < 75°N	118	1.13	161	14
	75°N < lat < 80°N	123	1.20	151	10
	80°N < lat < 85°N	138	0.96	166	11
	85°N < lat	149	0.73	175	8

414 Canadian Archipelago. North of the Svalbard islands and within a triangle, delineated by
 415 the 10°W and the 90°E meridians pointing towards the North pole, the algae-induced melt
 416 values are low.

422 3.3 Distinction between level ice and ridged ice

423 According to equations 2 and 3, we divide the ice into level ice and ridged ice. In
 424 Figure 11 we show the ridge density (number of ridges per km), the total thickness of ridged

425 ice, and differences in ice and snow thickness between level ice and the grid-averaged ice for
426 May. This is an illustrative example because in May the algal bloom for the grid-averaged
427 ice just started at higher latitudes. Moreover, in May there is still snow on the ice. The ridge
428 density (Figure 11a) is high, with values up to 20 ridges per kilometer in the western part of
429 the Nansen basin and particularly along the coast of Svalbard islands and Severnaya Zemlya
430 islands. Lower values (< 10 ridges per kilometer) are mainly found in the Beaufort Sea,
431 Laptev Sea and East Siberian Sea. The thickness of the ridged ice (Figure 11b) remains
432 between 4 to 6 m in almost the entire Arctic Ocean, values higher than 10 m are found
433 mainly in the Lincoln Sea and along the northern coast of Greenland. Both ice and snow
434 thickness have large variations in the longitudinal direction in the sector between 100° W
435 and 100° E, where also the number of ridges is higher.

436 We analyze algal bloom in relation to the under-ice light field for both level ice and
437 ridged ice in the different latitudinal sectors (Figure 12). In Table 5 we list (as done for
438 the grid-averaged ice) day of bloom onset, the corresponding value of PAR, and the day
439 and value of maximum chl *a* concentration. For level ice, day of bloom onset and day of
440 maximum biomass are delayed by 5 to 10 days compared to the grid-averaged ice (see Table
441 5), but they still occur 20 days (bloom onset) and 19 days (maximum biomass) earlier than
442 in ridged ice. Maximal biomass values for level ice are very close to the grid-averaged ice
443 values with differences no larger than $4 \text{ mg chl } a \text{ m}^{-2}$.

448 The light field under ridges is much weaker compared to the level ice and grid-averaged
449 ice (Figures 6 and 12). Nevertheless, a minimum light threshold value of $0.36 \mu\text{Einst m}^{-2} \text{ s}^{-1}$
450 [Mock and Gradinger, 1999] for algal growth is reached, and a small algal bloom develops.
451 The bloom under ridged ice in each latitudinal sector starts later than for the grid-averaged
452 ice. In the two southernmost sectors the delay is up to 30 days, whereas north of 80°N the
453 delay is 20 days. The maximum is also reached later with a delay of 20 to 40 days compared
454 to grid-averaged sea ice. Moreover, the southernmost band shows a slower growth with a
455 maximum biomass reached 10 days later than in the band $75^\circ\text{N} < \text{lat} < 80^\circ\text{N}$. The values
456 of maximum biomass are half of the grid-averaged and level ice values. In particular, the
457 maximum biomass under ridged ice in the latitudinal sector north of 85°N is smaller than
458 the values of maximum biomass in the other sectors, opposite to what happens in level ice
459 and grid-averaged ice.

460 In both level ice and ridged ice, nitrate increases during the first months of the year
 461 reaching values around 70 mg m^{-2} (Figure 13). Between mid April and mid June the nutri-
 462 ent concentrations start to decrease. Towards the beginning of July, the level ice is nutrient
 463 depleted in all the four latitudinal sectors. Under the ridged ice, nitrate concentrations are
 464 never exhausted.

467 In March and April, the total algae biomass (i.e., the chl *a* concentration integrated
 468 over the area of the grid cell and weighted by sea-ice concentration) of level ice is always
 469 larger than the total algae biomass of grid-averaged ice (Figure 14 shows the ratio of the
 470 two). In May, the total biomass ratio of level to grid-averaged ice is no longer larger than
 471 1 everywhere, but only in the latitudinal band $70^\circ\text{N} < \text{lat} < 75^\circ\text{N}$ and in part of the band
 472 $75^\circ\text{N} < \text{lat} < 80^\circ\text{N}$. For latitudes higher than 80°N , the ratio is always smaller than 1. In
 473 June, there is more biomass in the level ice than in the grid-averaged ice in all regions.

476 The ratio of ridged-ice algae to grid-averaged ice algae is almost always small, about
 477 0.05 to 0.1 (5% to 10%) in June and July (Figure 15), except for a band in July extending
 478 from the Beaufort Sea and Bering Strait to the Fram strait with values up to 0.5 (50%).

481 4 Discussion

482 4.1 Performance of SIMBA

483 The simulated spatial pattern of sea-ice algae concentrations at the end of summer
 484 resembles the pattern obtained from observations (BLROV). There is a belt of lower chl *a*
 485 concentration extending towards the sea ice edge within the eastern sector (Figure 4). In this
 486 area the model reproduces the values from observations (Table 4). The algae concentration
 487 increases towards the central Arctic. Here the modeled mean ice algae concentration and
 488 field measurements are different. North of 85°N , however, observations are in the range of
 489 modeled values. The latitudinal pattern of algae concentrations increasing from south to
 490 north was already observed in July-August 1994 [*Gosselin et al.*, 1997]. In particular, they
 491 report values of bottom sea-ice algal chl *a* concentrations (3 to $14 \text{ mg chl } a \text{ m}^{-2}$) in the area
 492 close to the North Pole, which are three times higher than in the latitudinal bands south of
 493 70°N . North of 85°N , particularly in the Eastern sector, model results agree with summer
 494 values of 1 to $7 \text{ mg chl } a \text{ m}^{-2}$ in 1991 [*Gradinger*, 1999]. In agreement with model results, low
 495 values of chl *a* concentrations ($< 1 \text{ mg chl } a \text{ m}^{-2}$) were also observed at the end of summer
 496 during a 1993 study in the Laptev Sea and north of Svalbard [*Gradinger and Zhang*, 1997],

497 in 1994 and 1995 in the Fram Strait and Greenland sea [*Gradinger et al.*, 1999; *Werner and*
498 *Gradinger*, 2002], in 1998 in the Chukchi plateau [*Melnikov et al.*, 2002], in 2002 in the Fram
499 Strait [*Schünemann and Werner*, 2005], in 2002 and 2003 in the Beaufort Gyre [*Gradinger*
500 *et al.*, 2005], and in 2005 in the Chukchi/Beaufort Sea [*Gradinger et al.*, 2010]. The only two
501 studies [*Lange et al.*, 2015, 2017] of sea-ice algae concentration in the Lincoln Sea are from
502 the spring season. *Lange et al.* [2015, 2017] show mean values of sea-ice algae concentration
503 for spring 2012 below $2 \text{ mg chl } a \text{ m}^{-2}$, where the model estimates a mean concentration
504 of $1.93 \text{ mg chl } a \text{ m}^{-2}$. Note that all studies cited above focus mainly on thicker ice, in
505 particular, we consider for our comparison only literature values for ice thicker than 1.5 m
506 to reduce the risk of measurements biased towards the thinner sea-ice classes.

507 What might be interpreted as a merely latitudinal dependency from observations alone,
508 has a different interpretation from our model results. Here the algae concentration follows a
509 latitudinal pattern on the Eastern side ($\sim 20^\circ\text{E}$ to 180°E , see Figure 4), but it also depends
510 strongly on thickness, which increases closer to the coast within the western sector. Analyz-
511 ing the total summer melt (Figure 5) we see a very similar pattern at the end of summer,
512 even though the correlation coefficients are small ($r < 0.2$). In particular, the very thick ice
513 in the Lincoln Sea has lower algal loss due to lower melt rates in this region [*Dupont*, 2012].

514 The algal bloom is initiated after PAR exceeds a lower limit (Figure 6, see also *Horner*
515 *and Schrader* [1982]; *Gosselin et al.* [1986]; *Mock and Gradinger* [1999]; *Lange et al.* [2015]).
516 The spatial distribution of the bloom onset (Figure 7) suggests that factors other than
517 latitude (i.e., incoming radiation, albedo, ice thickness and snow thickness) affect the spatial
518 distribution. It is, however, very difficult to decouple the effects of these single variables. For
519 example, the late bloom in the Lincoln sea can be explained by the large sea-ice thickness
520 values whereas the delay in the Kara Sea and Fram Strait is caused by the thicker snow
521 cover. Correlations of day of bloom onset with day of snow melt ($r = 0.19$) and with ice
522 thickness ($r = 0.22$) are weak but significant. A moderate correlation ($r = 0.57$) is found with
523 the snow thickness distribution. Such low correlation values are caused by the large area
524 considered and the large scale of variability of all variables controlling ice algal growth. The
525 correlation should be investigated at smaller scales because sea ice algae biomass in different
526 regions of the Arctic can have substantially different relationships with the physical sea ice
527 environment.

528 The maximum chl *a* concentration is also reached later in the higher latitude regions.
529 We compare our results with what is shown in *Leu et al.* [2015]. We look at the curves for
530 the stations in the two regions of interest and compare the day and value of maximum with
531 our results. From *Leu et al.* [2015] we infer a day of maximum biomass of 138 and 146 for
532 the two regions $70^{\circ}\text{N} < \text{lat} < 75^{\circ}\text{N}$ and $75^{\circ}\text{N} < \text{lat} < 80^{\circ}\text{N}$ with maxima of ~ 14.5 and ~ 22.5
533 $\text{mg chl } a \text{ m}^{-2}$ respectively. Our results for day of maximum biomass are 20 and 14 days
534 earlier, respectively (Table 5), and show a higher maximum value of chl *a* concentrations
535 (more than double in the southernmost latitudinal band). Since we discard a latitudinal
536 effect in the comparison, further investigation to assess the cause of the earlier modeled day
537 of maximum biomass should be addressed (but not performed in the present study). We
538 may speculate that the spatial coverage of observations is heavily biased towards coastal
539 regions and landfast sea ice, which may have different nutrient regimes and dynamic sea-ice
540 processes. Moreover, the simplified nutrient initialization used in the present study can lead
541 to overestimating the maximum biomass values (see Section 4.2).

542 **4.2 Effects of different initial conditions**

543 We use the algal bloom as a key process to compare different scenarios listed in Table
544 3 and investigate the effect of different initial conditions. Between scenarios R2, R4, R6
545 and R8, the differences in bloom onset are only ± 2 days. The largest difference between
546 these scenarios is the maximum biomass reached during the bloom. Nitrate availability in
547 winter and spring determines the total primary production in the late spring so that highest
548 biomass peaks are reached in runs with higher initial nutrient concentration. This shows the
549 key role of nutrient concentrations in winter and thus the importance of having observations
550 collected before the algal bloom. Of particular interest is scenario R0, which has the lowest
551 maximum biomass, but also shows an earlier bloom period (40 days earlier). Furthermore,
552 the decay is slower for R0 compared to other scenarios, so the minimum is reached between
553 August and September, which is consistent with other runs. This means that the conditions
554 at the end of summer are similar for all scenarios, as can be seen in Table 3.

555 **4.3 Effects caused by ice algae on ice and ocean**

556 Ice algae can have an influence on both ocean and sea ice. The shading created by sea-
557 ice algae can delay the under-ice phytoplankton bloom, thus further extending the thriving
558 window for sympagic and pelagic grazers [*Jin et al.*, 2012; *Tremblay et al.*, 2008]. Our

559 results show that the shading effect due to sea-ice algae differs according to the different
560 latitudinal sectors. Between 70°N and 80°N, ice algae keep the light level around the
561 mean threshold so that some growth is possible for under-ice phytoplankton. North of
562 80°N the light level is under the threshold value due to the shading effect, thus under-ice
563 phytoplankton bloom may be delayed by up to ~40 days, if not completely prevented as
564 shown by Dupont [2012]. Such shading effects may add to the shading already caused by
565 ice and snow on the ocean surface, thus further delaying the phytoplankton blooms under
566 the ice compared to the blooms in open water [Arrigo *et al.*, 2012]. However, the presence
567 of sea ice algae can have other effects on phytoplankton growth. Such effects include, e.g.,
568 uptake and remineralization of nutrients by sea-ice algae, but their investigation requires
569 coupling to an ocean biogeochemical model. Thus, the results presented here for the effects
570 of ice algae on under ice phytoplankton blooms should be corroborated with a coupled ice
571 algae–phytoplankton model.

572 The ice algae-induced melt, integrated from April to August, ranges from 0 to 2 cm and
573 agrees with previous studies [Zeebe *et al.*, 1996]. Ice algae induced melt is much smaller than
574 the range of variability of the physically induced melt (0 to 1.5 m) and thus negligible for
575 the physical system. Nevertheless, this positive feedback mechanisms can have measurable
576 effects in long term simulations. Moreover, the total ice algae induced melt can be important
577 for the algae layer, which could be eroded by the melt induced by the ice algae.

578 **4.4 Level ice and ridged ice**

579 After dividing sea ice into level ice and ridged ice based on the deformation energy and
580 sail density, resulting level ice is thinner than the grid-averaged ice, but it has a thicker snow
581 cover (Figure 11). These differences are reflected in light transmission and algae phenology.
582 In the presence of snow, there is less light under level ice than under the grid-averaged ice,
583 but after all snow is melted, there is more light under level ice because of thinner ice. Since
584 the amount of nutrients is the same, the maximum chl *a* concentration is very similar, mostly
585 because the system is determined by initial conditions for nutrients (Section 4.2 and Table
586 5). Nevertheless, the presence of thicker snow has an important influence on the timing
587 of algal growth. Figure 14 shows that in April there are more algae associated with the
588 grid-averaged ice. This ratio changes in May, when in the marginal ice zone the level-ice
589 algae are close to the maximum of the bloom, whereas the grid-averaged ice algae start to
590 decay. In June, algae associated to the grid-averaged sea ice are already decreasing whereas

591 the amount of biomass associated with level ice is still high. Thus changes in the snow cover,
592 rather than in ice thickness, have a large effect on the timing of the algal bloom.

593 Ridges create a very special environment for ice algae [*Kuparinen et al.*, 2007; *Vancop-*
594 *penolle et al.*, 2013]. As such, they show a pattern for both physical factors and algal growth
595 different from level ice and grid-averaged ice. The ridge-associated algae can constitute more
596 than 50 per cent of the total algae that grow under the grid-averaged ice (Figure 15). Due
597 to the specific light conditions, the bloom under ridged ice appears later in the season than
598 for grid-averaged ice or level ice, thus it can provide an extra source of carbon towards the
599 end of the feeding season when other food sources are already depleted. We stress that our
600 parameterization does not provide an accurate representation of the structural and geomet-
601 rical properties of ridges. Potential effects along the ridge edges, where ridges are thinner
602 and might let more light pass through due to horizontal scattering, are not included in this
603 work. Moreover, ridges can incorporate water pockets during formation, which could repre-
604 sent a nutrient reservoir for algae. Finally, scattering and absorption processes in ridges are
605 not yet parameterized.

606 The distinction between level and ridged ice classes shows that with the grid-averaged
607 ice only, it may not be possible to accurately represent the actual timing of algal growth
608 and bloom. Based on our modeling results, in combination with floe-scale observations
609 (BLROV) we recommend that different ice classes should be considered when the aim is to
610 model algae content and evolution.

611 **5 Conclusions and outlook**

612 A new Arctic-wide sea-ice algal model coupled to a sea-ice–ocean general circulation
613 model, helps interpreting observations of ice algal biomass. In spite of its simplicity, the
614 new model reproduces part of the observed distributions of biomass, in particular, the
615 latitudinal pattern in an eastern sector south of 80°N. In other areas, snow and ice thickness
616 affect light availability and thus algal growth in a complicated manner. In this situation,
617 the interpretation of observations is difficult, because often the available data sets do not
618 provide all the pieces of information required to attribute the phenology of sea-ice algae to
619 physical constraints.

620 Ice-algae phenology is driven by different physical factors that vary with season and
621 region. Ice-algal blooms are delayed with latitude (i.e. light) and affected by snow and ice

622 thickness. The bloom peak values depend on initial conditions, especially of nutrients. In
623 all cases, nutrient limitation terminates the bloom and by the end of summer the algae
624 concentration pattern resembles that of the basal melt. A better spatial and temporal
625 coverage of observations, ideally during the key transition periods between the onset of the
626 bloom until the end of summer, is required to validate the accuracy of these numerical model
627 experiments for the entire period.

628 The shading effect due to an algae layer and the increased melting due to energy
629 released by algae as heat are two mechanisms that feed back into the physical sea-ice and
630 ocean system. The shading effect is not important south of 80°N, but north of 80°N it can
631 delay the under-ice phytoplankton bloom by up to 40 days. The release of heat by ice algae
632 can contribute to an overall annual sea ice melt of up to 2 cm, much smaller than the total
633 melt due to physical processes.

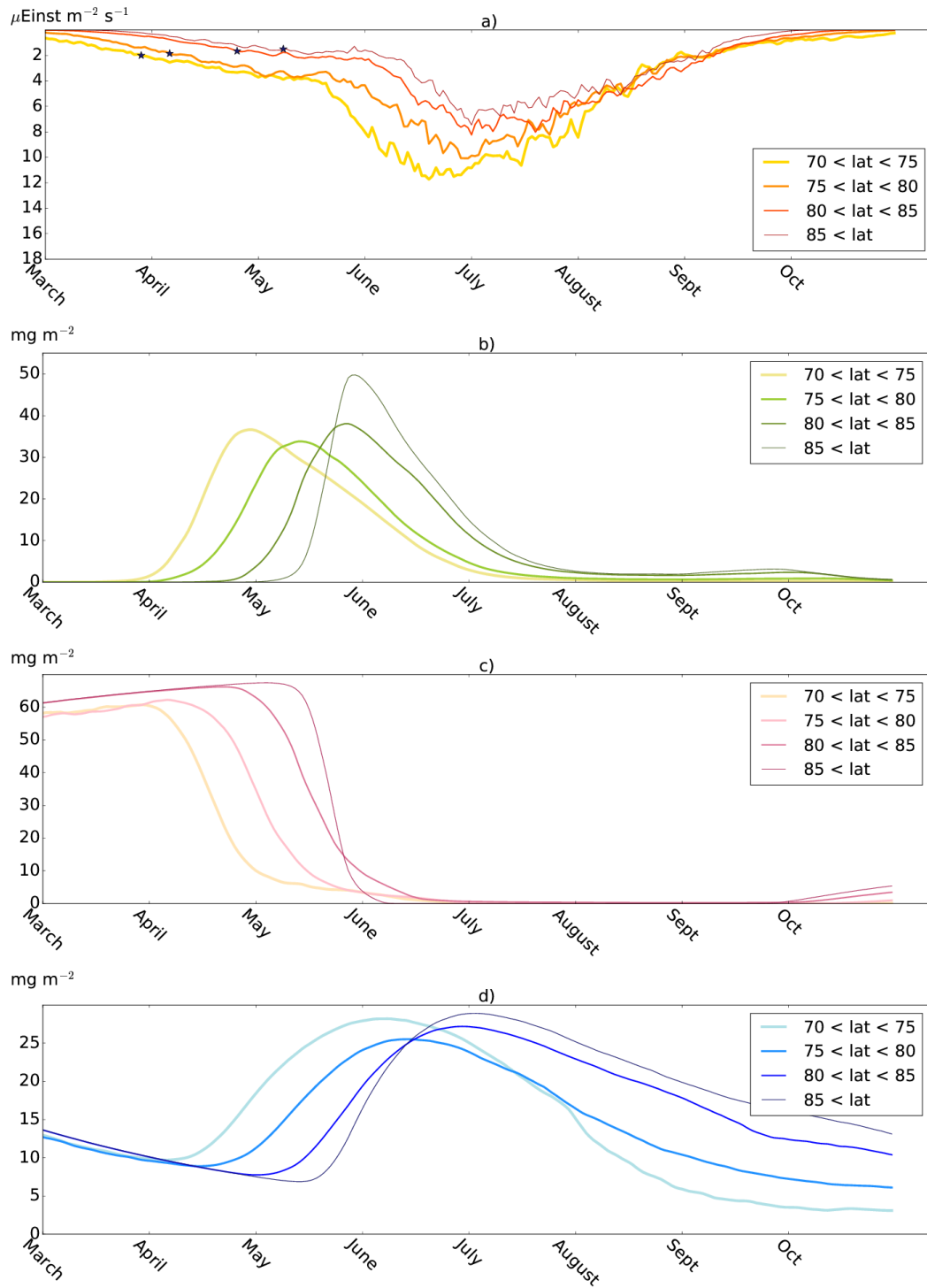
634 The algal bloom and decay are functions of the physical properties of level and ridged
635 ice. Level ice is thinner than grid-cell averaged ice, but the redistribution of snow results in
636 more snow on level ice. This extra snow delays the onset of the algal bloom under level ice.
637 Ridged ice can host algae communities that grow and support primary production when a
638 minimum value of under-ice light is reached in summer. Thus, they represent an additional
639 food source for sympagic and pelagic species during the end of summer when other food
640 resources are limited. Our results show that different sea-ice classes might be useful in
641 properly representing sea-ice algae spatial distribution and phenology.

642 The model is at an early stage of development and is lacking the representation of
643 some important processes. In particular, the exchange of nutrients with the underlying
644 ocean is an important term to sustain the growth and survival of bottom sea-ice algae after
645 nutrients that have been captured within the sea-ice matrix at the time of freezing are
646 depleted. For multi-year simulations, which allow to assess interannual changes in sea-ice
647 algae concentrations, the initialization of nutrients and ice algae at ice formation need to
648 be parameterized. The model could further be improved by coupling the biogeochemical
649 processes at the bottom of sea ice to those within the upper ocean, that is to an ocean-
650 biogeochemical module.

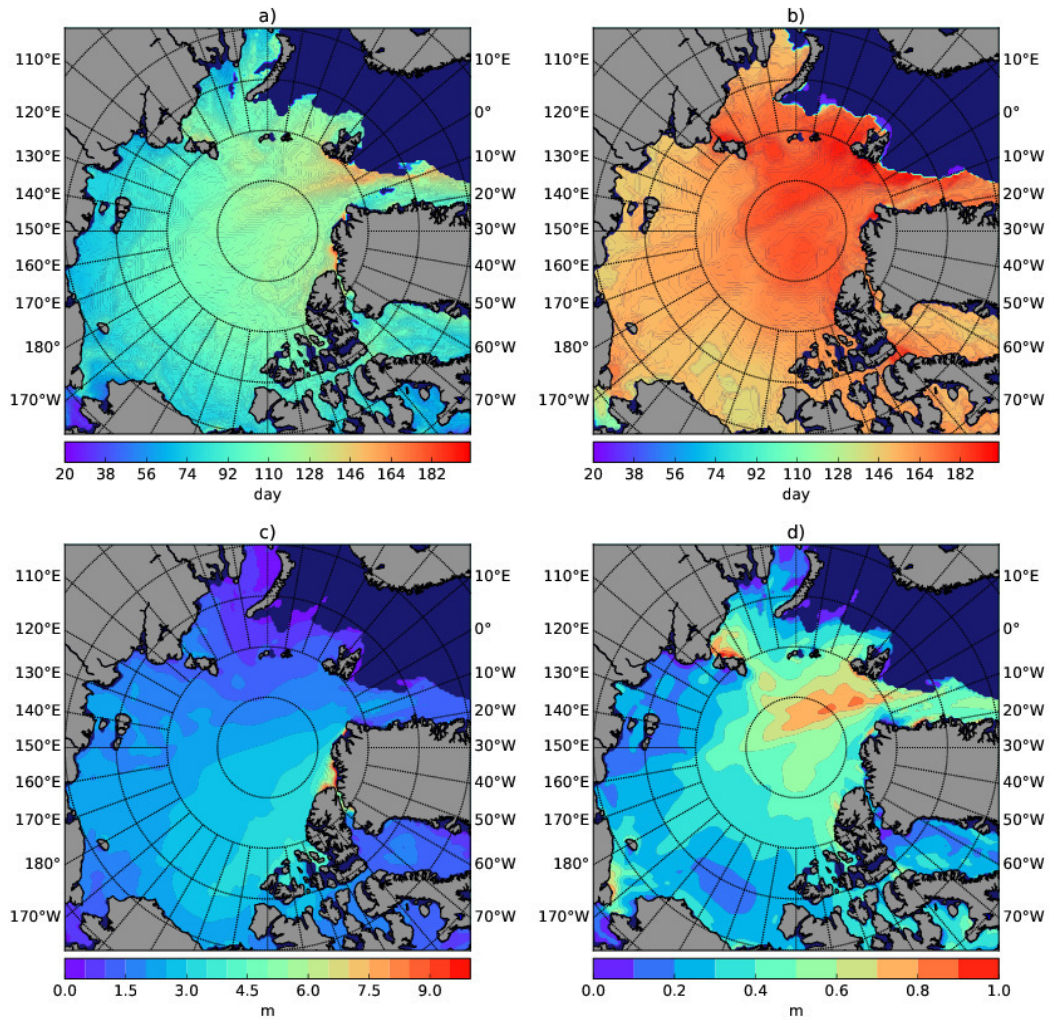
651 **Acknowledgments**

652 This study is part of the Helmholtz Association Young Investigators Group *Iceflux*: Ice-

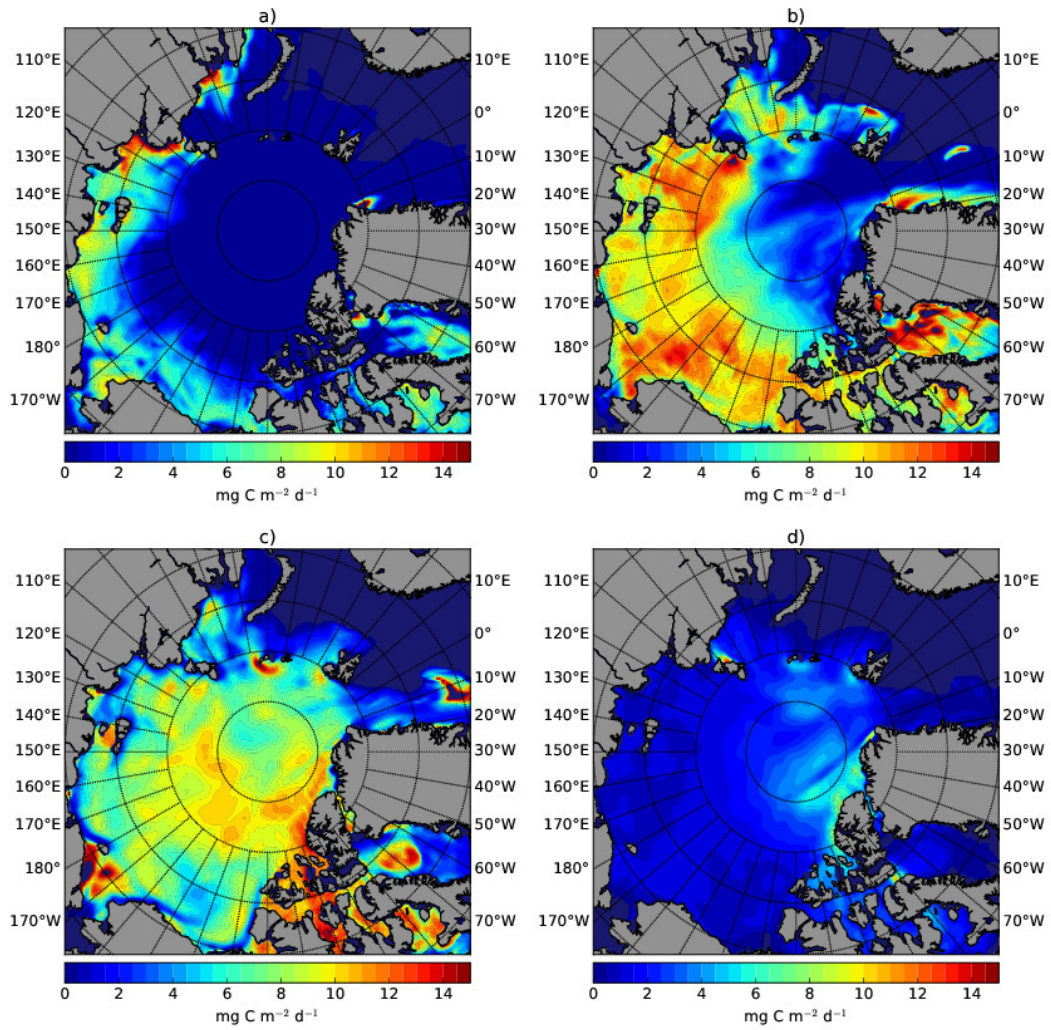
653 ecosystem carbon flux in polar oceans (VH-NG-800). We sincerely thank two anonymous
654 reviewers for the constructive comments on previous versions of the present manuscript.
655 The general MITgcm code is available at <http://mitgcm.org/>. The code for SIMBA and the
656 routines used for the analysis are available upon request at giulia.castellani@awi.de.



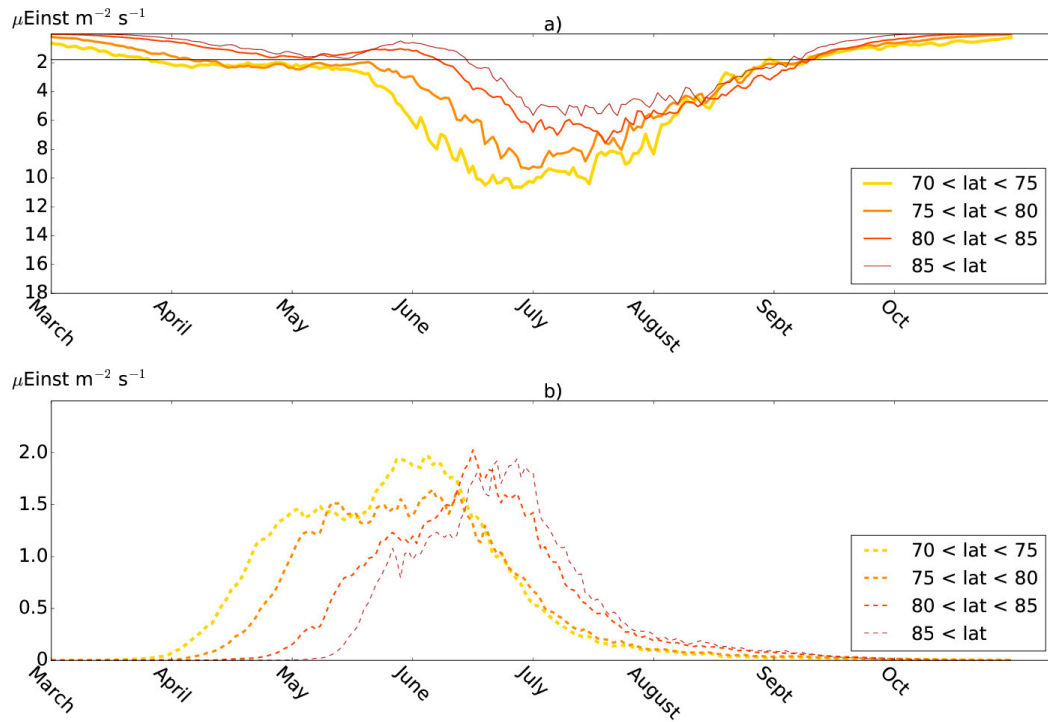
345 **Figure 6.** Model simulation between March and November for: a) under-ice light (positive
 346 downward) for the grid-averaged sea ice, b) sea-ice algal bloom, c) nutrient concentration and d)
 347 detritus concentration. Results are presented as averages over four latitudinal sectors as shown in
 348 Figure 2. The stars in panel a) identify the onset of algal bloom in each latitudinal band (values
 349 are listed in Table 5).



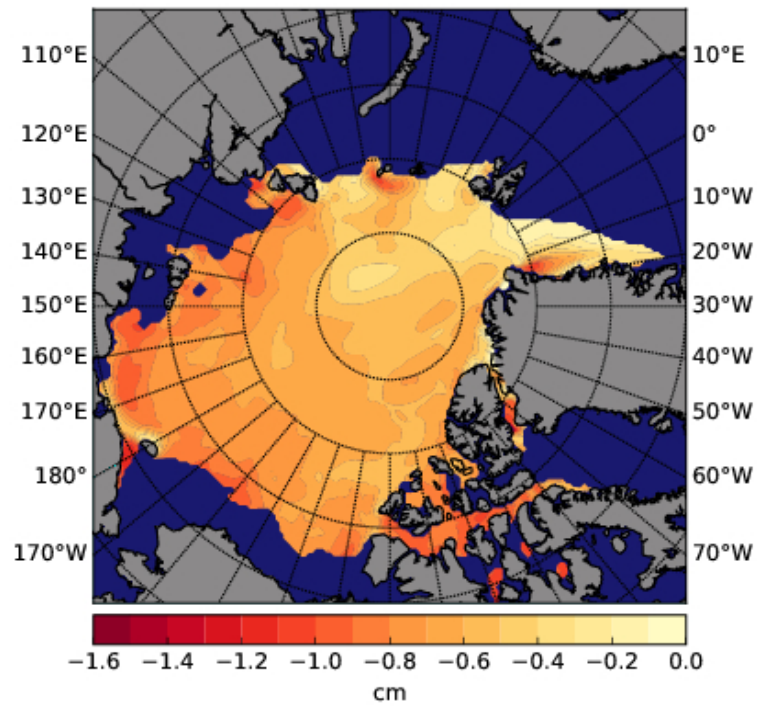
386 **Figure 7.** Maps for the Arctic showing a) bloom onset as the day from the beginning of January,
 387 b) complete snow melt ($H_s = 0$) as the day from the beginning of January, c) ice thickness at the
 388 day of bloom onset and d) snow thickness at the day of bloom onset.



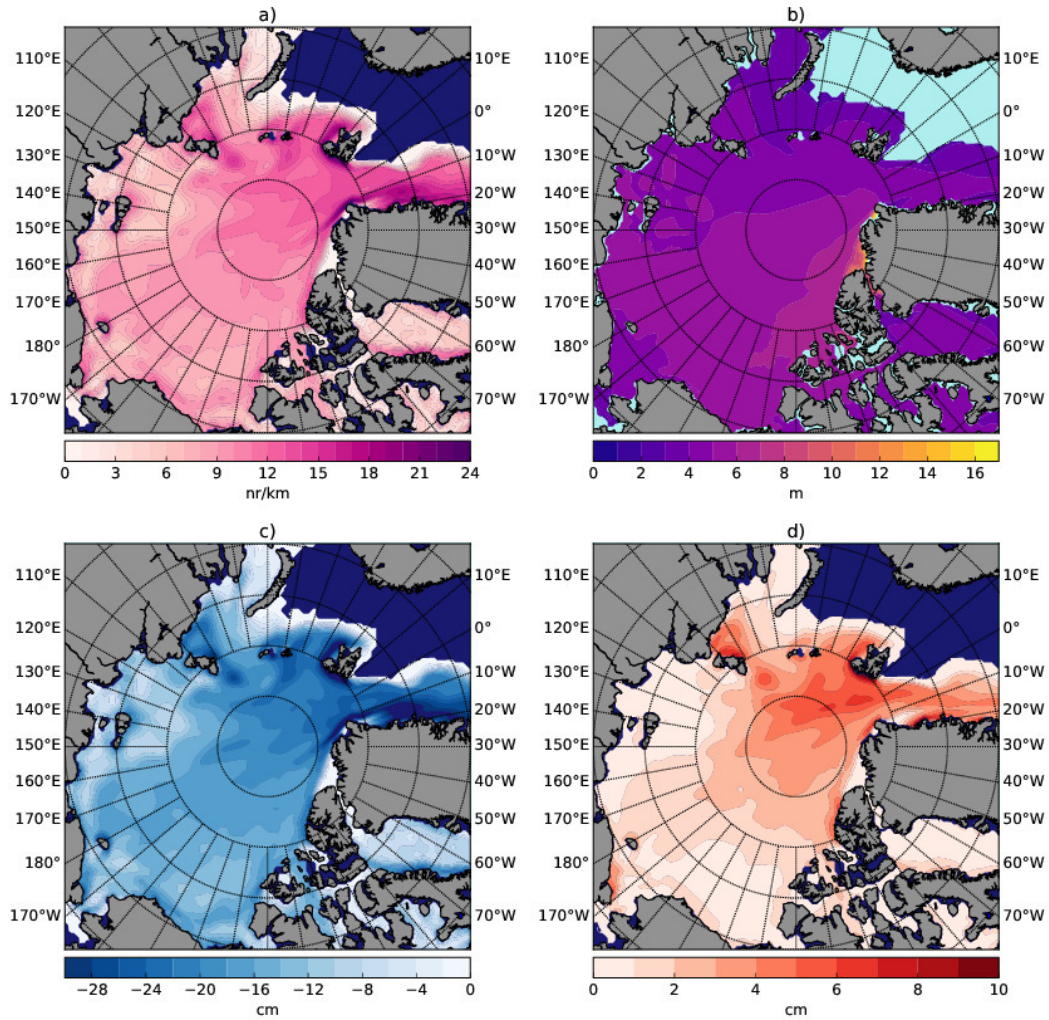
394 **Figure 8.** Maps of monthly averaged sea-ice algae NPP for a) April, b) May, c) June and d)
 395 July 2012.



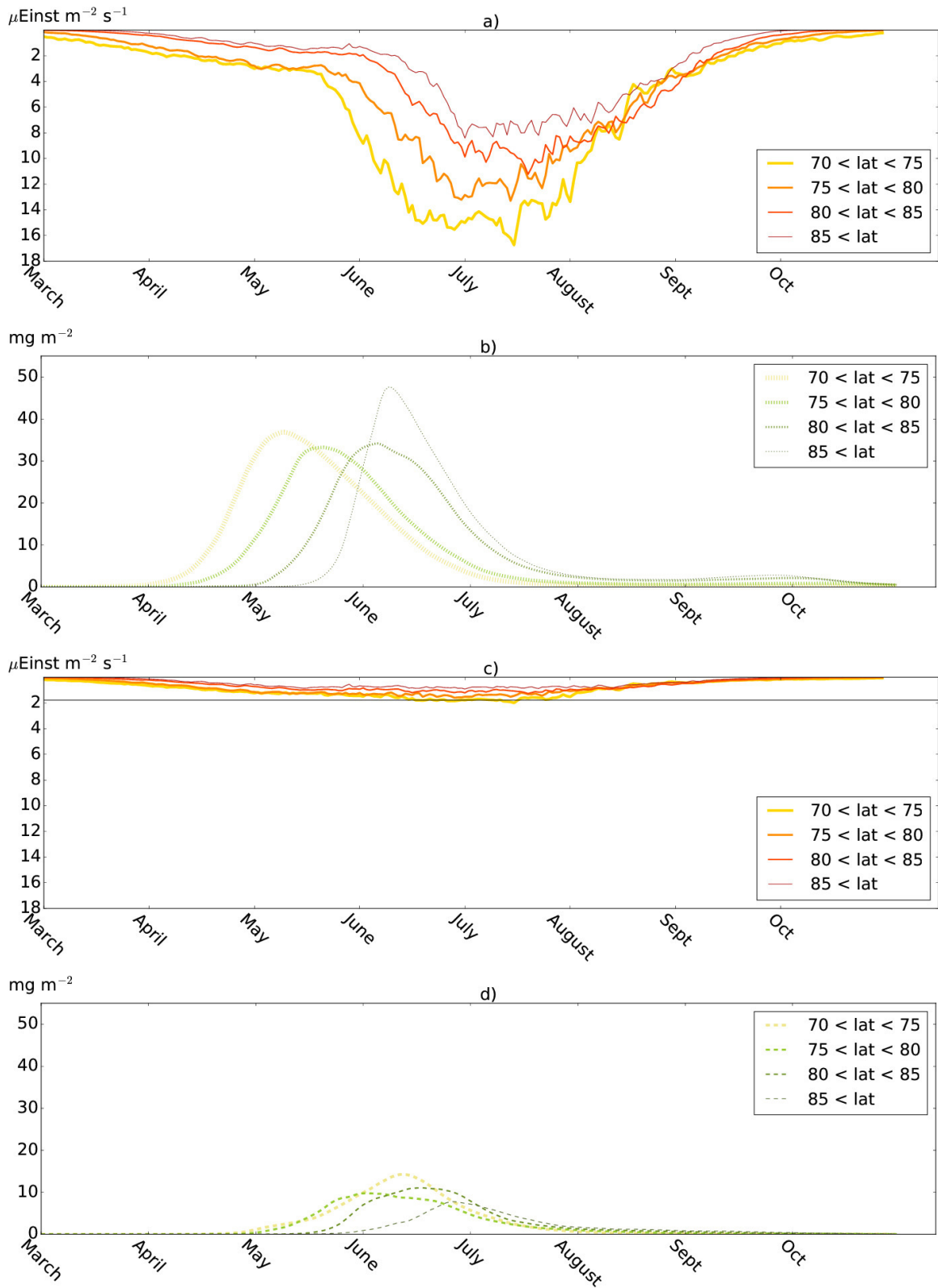
405 **Figure 9.** Plots of: a) under-ice light when the shading effect due to sea-ice algae is considered,
 406 and b) differences between under ice light computed without algae shading (Figure 6a) and under-
 407 ice light computed considering the shading effect due to algae. The horizontal gray line in panel a)
 408 at $1.78 \mu\text{Einst m}^{-2} \text{s}^{-1}$ represents the limit for algal bloom as average of values indicated by stars
 409 in Figure 6a.



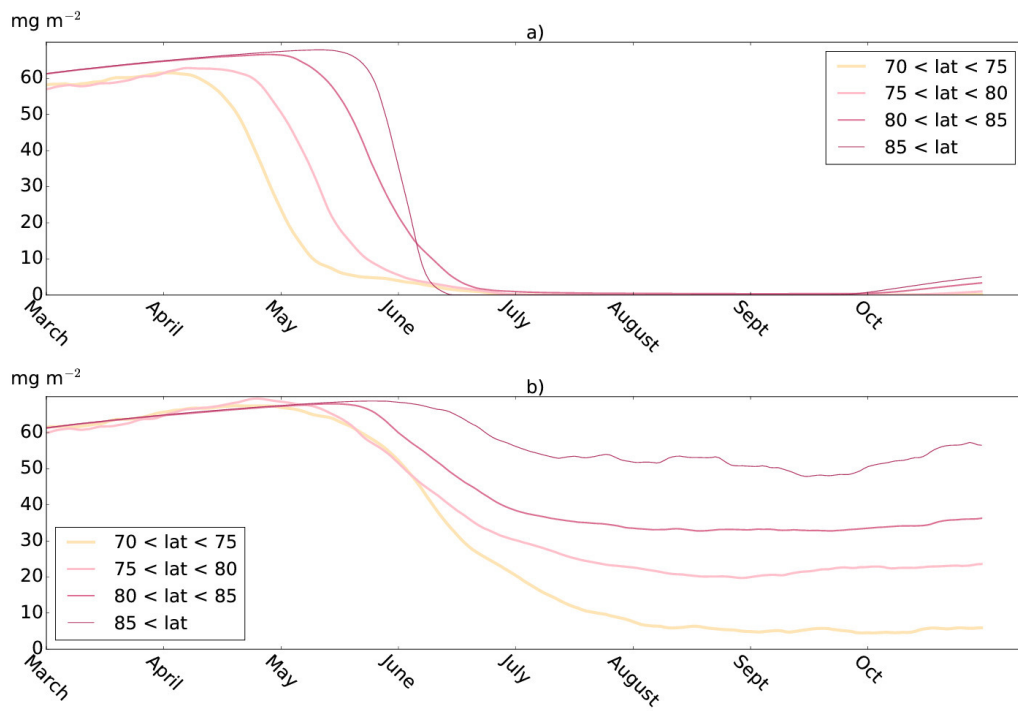
417 **Figure 10.** Integrated summer basal ice melt over the period April to September 2012 caused
418 by heat released by sea-ice algae.



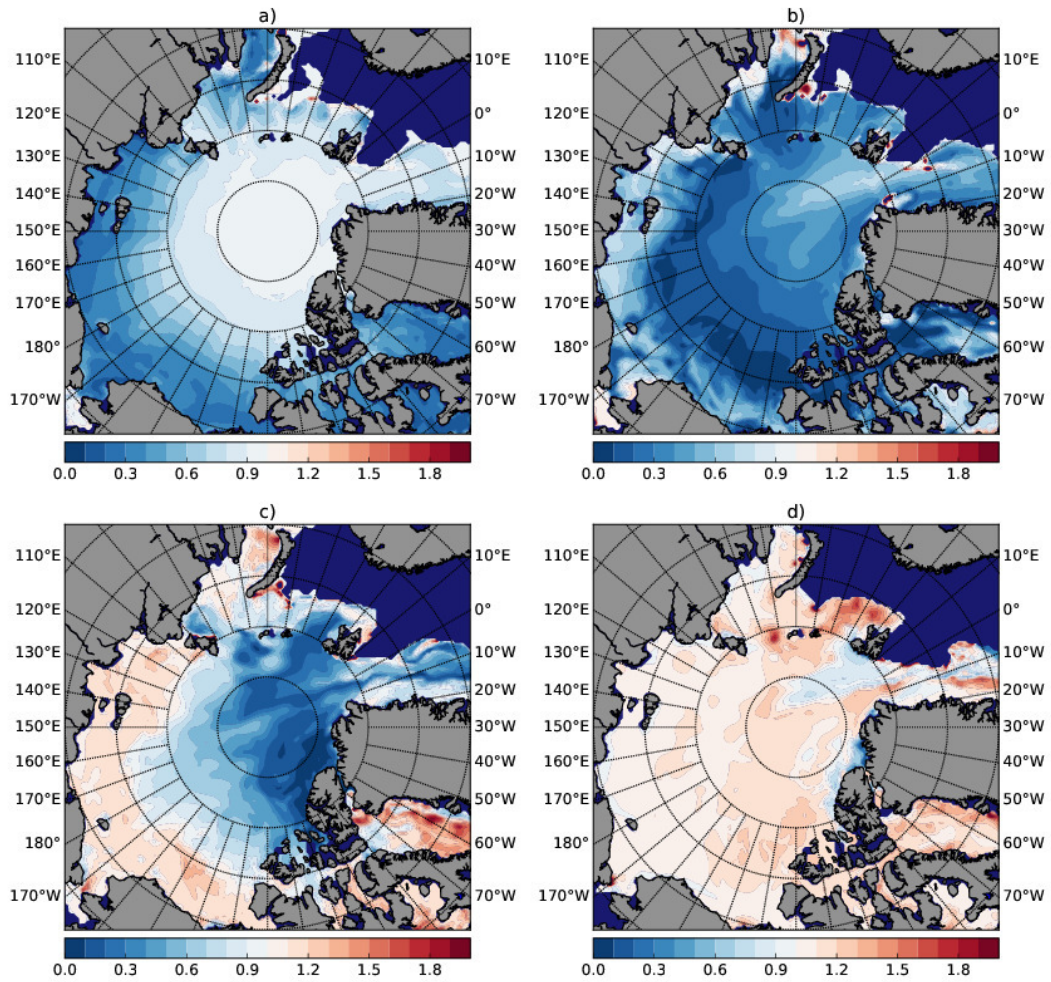
419 **Figure 11.** Maps of May averages for: a) ridge density, b) thickness of ridged ice, c) differences
 420 in ice thickness between level ice and grid-averaged ice, and d) snow thickness differences between
 421 level ice and the grid-averaged ice.



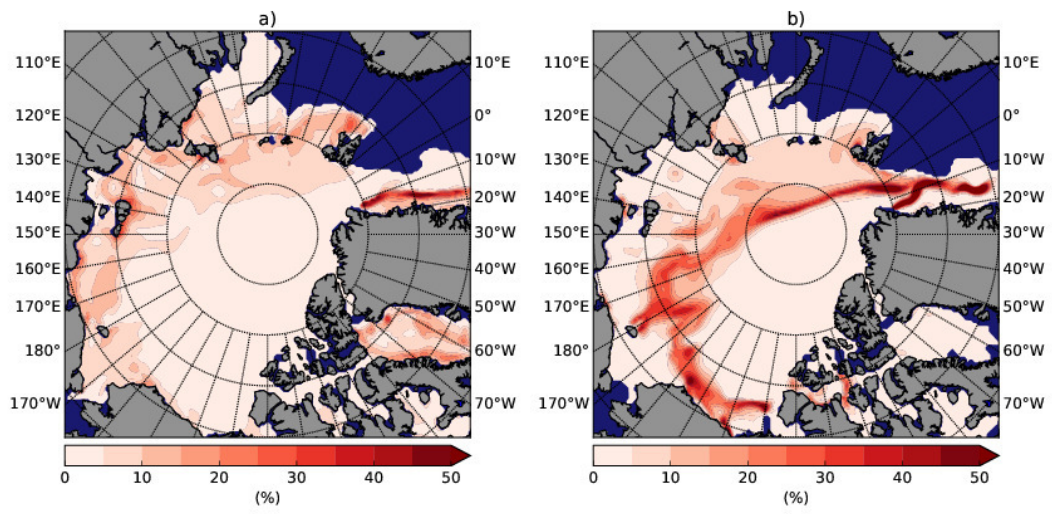
444 **Figure 12.** Level ice: a) Under-ice light and b) algae evolution. Ridged ice: c) Under-ice light
 445 and d) algae evolution. The horizontal gray line in panel c) represents the limit value for PAR of
 446 1.78 $\mu\text{Einst m}^{-2} \text{s}^{-1}$ inferred by Figure 6. Quantities are averaged over the four latitudinal sectors
 447 shown in Figure 2.



465 **Figure 13.** Nutrient evolution for a) level ice, and b) ridged ice in the four latitudinal sectors
 466 shown in Figure 2.



474 **Figure 14.** Ratio between grid integrated level-ice algae and grid-averaged ice algae in a) March,
475 b) April, c) May and d) June 2012.



479 **Figure 15.** Grid integrated ridged-ice algal biomass as percent of grid-averaged ice algae for a)
480 June and b) July.

References

657

658 Arrigo, K. R., and G. L. van Dijken (2011), Secular trends in Arctic Ocean net primary pro-
659 duction, *Journal of Geophysical Research: Oceans*, *116*(C9), doi:10.1029/2011JC007151,
660 c09011.

661 Arrigo, K. R., J. N. Kremer, and C. W. Sullivan (1993), A simulated Antarctic ast
662 ice ecosystem, *Journal of Geophysical Research: Oceans*, *98*(C4), 6929–6946, doi:
663 10.1029/93JC00141.

664 Arrigo, K. R., D. L. Worthen, M. P. Lizotte, P. Dixon, and G. Dieckmann
665 (1997), Primary Production in Antarctic Sea Ice, *Science*, *276*(5311), 394–397, doi:
666 10.1126/science.276.5311.394.

667 Arrigo, K. R., D. K. Perovich, R. S. Pickart, Z. W. Brown, G. L. van Dijken, K. E. Lowry,
668 M. M. Mills, M. A. Palmer, W. M. Balch, F. Bahr, N. R. Bates, C. Benitez-Nelson,
669 B. Bowler, E. Brownlee, J. K. Ehn, K. E. Frey, R. Garley, S. R. Laney, L. Lubelczyk,
670 J. Mathis, A. Matsuoaka, B. G. Mitchell, G. W. K. Moore, E. Ortega-Retuerta, S. Pal,
671 C. M. Polashenski, R. A. Reynolds, B. Schieber, H. M. Sosik, M. Stephens, and J. H.
672 Swift (2012), Massive Phytoplankton Blooms Under Arctic Sea Ice, *Science*, *336*(6087),
673 1408–1408, doi:10.1126/science.1215065.

674 Belém, A. L. (2002), Modeling physical and biological processes in Antarctic sea ice, Ph.D.
675 thesis, University of Bremen.

676 Castellani, G. (2014), Momentum exchange between atmosphere, sea ice and ocean, Ph.D.
677 thesis, Jacobs University.

678 Castellani, G., C. Lüpkes, S. Hendricks, and R. Gerdes (2014), Variability of Arctic sea ice
679 topography and its impact on the atmospheric surface drag, *J. Geophys. Res. Oceans*,
680 *119*, 6743–6762, doi:10.1002/2013JC009,712.

681 Castro-Morales, K., F. Kauker, M. Losch, S. Hendricks, K. Riemann-Campe, and
682 R. Gerdes (2014), Sensitivity of simulated Arctic sea ice to realistic ice thickness
683 distributions and snow parameterizations, *J. Geophys. Res. Oceans*, *119*, 559–571,
684 doi:10.1002/2013JC009,342.

685 Comiso, J. C. (2012), Large Decadal Decline of the Arctic Multiyear Ice Cover, *Journal of*
686 *Climate*, *25*(4), 1176–1193, doi:10.1175/JCLI-D-11-00113.1.

687 Cota, G. F., S. J. Prinsenberg, E. B. Bennett, J. W. Loder, M. R. Lewis, J. L. Anning,
688 N. H. F. Watson, and L. R. Harris (1987), Nutrient fluxes during extended blooms
689 of Arctic ice algae, *Journal of Geophysical Research: Oceans*, *92*(C2), 1951–1962, doi:

- 690 10.1029/JC092iC02p01951.
- 691 Deal, C., M. Jin, S. Elliott, E. Hunke, M. Maltrud, and N. Jeffery (2011), Large-scale
692 modeling of primary production and ice algal biomass within arctic sea ice in 1992, *Journal*
693 *of Geophysical Research: Oceans*, *116*(C7), doi:10.1029/2010JC006409, c07004.
- 694 Dupont, F. (2012), Impact of sea-ice biology on overall primary production in a biophysical
695 model of the pan-Arctic Ocean, *Journal of Geophysical Research: Oceans*, *117*(C8), doi:
696 10.1029/2011JC006983, c00D17.
- 697 Fernández-Méndez, M., C. Katlein, B. Rabe, M. Nicolaus, I. Peeken, K. Bakker, H. Flores,
698 and A. Boetius (2015), Photosynthetic production in the central Arctic Ocean during the
699 record sea-ice minimum in 2012, *Biogeosciences*, *12*(11), 3525–3549, doi:10.5194/bg-12-
700 3525-2015.
- 701 Fernández-Méndez, M., K. A. Turk-Kubo, P. L. Buttigieg, J. Z. Rapp, T. Krumpfen, J. P.
702 Zehr, and A. Boetius (2016), Diazotroph Diversity in the Sea Ice, Melt Ponds, and Surface
703 Waters of the Eurasian Basin of the Central Arctic Ocean, *Frontiers in Microbiology*, *7*.
- 704 Frouin, R., and R. T. Pinker (1995), Estimating photosynthetically active radiation (PAR)
705 at the Earth’s surface from satellite observations, *Remote Sensing of Environment*, *51*,
706 98–107.
- 707 Gosselin, M., L. Legendre, J.-C. Therriault, S. Demers, and M. Rochet (1986), Physical
708 control of the horizontal patchiness of sea-ice microalgae, *Marine Ecology Progress Series*,
709 *29*, 289–298.
- 710 Gosselin, M., M. Levasseur, P. A. Wheeler, R. A. Horner, and B. C. Booth (1997), New
711 measurements of phytoplankton and ice algal production in the Arctic Ocean, *Deep Sea*
712 *Research II*, *44*(8), 1623–1644.
- 713 Gradinger, R. (1999), Vertical fine structure of the biomass and composition of algal com-
714 munities in Arctic pack ice, *Marine Biology*, *133*(4), 745–754, doi:10.1007/s002270050516.
- 715 Gradinger, R., and Q. Zhang (1997), Vertical distribution of bacteria in Arctic sea ice from
716 the Barents and Laptev Seas, *Polar Biology*, *17*(5), 448–454, doi:10.1007/s003000050139.
- 717 Gradinger, R., C. Friedrich, and M. Spindler (1999), Abundance, biomass and composition
718 of the sea ice biota of the Greenland Sea pack ice, *Deep Sea Research Part II: Topical*
719 *Studies in Oceanography*, *46*(6–7), 1457–1472, doi:10.1016/S0967-0645(99)00030-2.
- 720 Gradinger, R., B. Bluhm, and K. Iken (2010), Arctic sea-ice ridges—Safe heavens for sea-ice
721 fauna during periods of extreme ice melt?, *Deep Sea Research Part II: Topical Studies*
722 *in Oceanography*, *57*(1–2), 86–95, doi:10.1016/j.dsr2.2009.08.008, observations and Ex-

- 723 ploration of the Arctic's Canada Basin and the Chukchi Sea: the Hidden Ocean and
724 {RUSALCA} Expeditions.
- 725 Gradinger, R. R., K. Meiners, G. Plumley, Q. Zhang, and B. A. Bluhm (2005), Abundance
726 and composition of the sea-ice meiofauna in off-shore pack ice of the Beaufort Gyre in
727 summer 2002 and 2003, *Polar Biology*, *28*(3), 171–181, doi:10.1007/s00300-004-0674-5.
- 728 Grenfell, T. C., and G. A. Maykut (1977), The optical properties of ice and snow in the
729 Arctic basin, *Journal of Glaciology*, *18*(80).
- 730 Grossi, S., S. Kottmeier, R. Moe, G. Taylor, and C. W. Sullivan (1987), Sea ice microbial
731 communities. Growth and primary production in bottom ice under graded snow cover.,
732 *Marine Ecology Progress Series*, *35*, 153–164.
- 733 Haas, C., A. Pfaffling, S. Hendricks, L. Rabenstein, J.-L. Etienne, and I. Rigor (2008),
734 Reduced ice thickness in Arctic Transpolar Drift favors rapid ice retreat, *Geophys. Res.*
735 *Lett.*, *35*(L17501), doi:10.1029/2008GL034,457.
- 736 Hibler, W. D. I. (1979), A dynamic thermodynamic sea ice model, *J. Phys. Oceanogr.*, *9*,
737 815–846.
- 738 Hibler, W. D. I. (1980), Modeling a variable thickness sea ice cover, *Mon. Weather Rev.*,
739 *108*, 1943–1973.
- 740 Hibler, W. D. I. (1984), The role of sea ice dynamics in modeling CO₂ increases, in *Cli-*
741 *mate Processes and Climate sensitivity*, edited by J. E. Hansen and T. Takahashi, AGU,
742 Washington, D. C., doi: 10.1029/GM029p0238.
- 743 Horner, R. A., and G. C. Schrader (1982), Relative Contributions of Ice Algae, Phytoplank-
744 ton, and Benthic Microalgae to Primary Production in Nearshore Regions of the Beaufort
745 Sea, *ARCTIC*, *35*(4), 485–503.
- 746 Iacozza, J., and D. G. Barber (1999), An examination of the distribution of snow on sea-ice,
747 *Atmosphere-Ocean*, *37*(1), 21–51.
- 748 Ivanova, N., O. M. Johannessen, L. T. Pedersen, IEEE-Members, and R. T. Tonboe (2014),
749 Retrieval of Arctic Sea Ice Parameters by Satellite Passive Microwave Sensors: A Com-
750 parison of Eleven Sea Ice Concentration Algorithms, *IEEE Transactions on Geoscience*
751 *and Remote Sensing*, *52*(11).
- 752 Ji, R., M. Jin, and Ø. Varpe (2013), Sea ice phenology and timing of primary pro-
753 duction pulses in the Arctic Ocean, *Global Change Biology*, *19*(3), 734–741, doi:
754 10.1111/gcb.12074.

- 755 Jin, M., J. C. Deal, J. Wang, K.-H. Shin, N. Tanaka, T. E. Whitledge, S. H. Lee, and R. R.
756 Gradinger (2006), Controls of the landfast ice-ocean ecosystem offshore Barrow, Alaska,
757 *Annals of Glaciology*, *44*, 63–72.
- 758 Jin, M., C. Deal, S. H. Lee, S. Elliott, E. Hunke, M. Maltrud, and N. Jeffery (2012),
759 Investigation of Arctic sea ice and ocean primary production for the period 1992–2007
760 using a 3-D global ice–ocean ecosystem model, *Deep Sea Research II*, *81*.
- 761 Kirk, J. T. O. (1983), Light and photosynthesis in aquatic ecosystems, *Cambridge Univ.*
762 *Press, New York*, (1), 401.
- 763 Kohlbach, D., M. Graeve, B. A. Lange, C. David, I. Peeken, and H. Flores (2016), The
764 importance of ice algae-produced carbon in the central Arctic Ocean ecosystem: Food web
765 relationships revealed by lipid and stable isotope analyses, *Limnology and Oceanography*,
766 *61*(6), 2027–2044, doi:10.1002/lno.10351.
- 767 Kohlbach, D., F. L. Schaafsma, M. Graeve, B. Lebreton, B. A. Lange, C. David,
768 M. Vortkamp, and H. Flores (2017), Strong linkage of polar cod (*Boreogadus saida*) to sea
769 ice algae-produced carbon: evidence from stomach content, fatty acid and stable isotope
770 analyses., *Progress in Oceanography*, *152*, 62–74, doi:10.1016/j.pocean.2017.02.003.
- 771 Kuparinen, J., H. Kuosa, A. Andersson, R. Autio, M. A. Granskog, J. Ikävalko, H. Kaar-
772 tokallio, K. Karell, E. Leskinen, J. Piiparinen, J. M. Rintala, and J. Tuomainen (2007),
773 Role of sea-ice biota in nutrient and organic material cycles in the northern Baltic Sea,
774 *Ambio*, *36*(2-3), 149–154.
- 775 Kwok, R., and D. A. Rothrock (2009), Decline in Arctic sea ice thickness from submarine
776 and ICESat records, *Geophys. Res. Lett.*, *36*(15)(L15501).
- 777 Kwok, R., G. F. Cunningham, M. Wensnahan, I. Rigor, H. J. Zwally, and D. Yi (2009),
778 Thinning and volume loss of the Arctic Ocean sea ice cover: 2003–2008, *Journal of Geo-*
779 *physical Research: Oceans*, *114*(C7), doi:10.1029/2009JC005312, e07005.
- 780 Lange, B. A., C. Michel, J. F. Beckers, J. A. Casey, H. Flores, I. Hatam, G. Meisterhans,
781 A. Niemi, and C. Haas (2015), Comparing Springtime Ice-Algal Chlorophyll a and Phys-
782 ical Properties of Multi-Year and First-Year Sea Ice from the Lincoln Sea, *PLoS ONE*,
783 *10*(4), e0122418, doi:10.1371/journal.pone.0122418.
- 784 Lange, B. A., C. Katlein, M. Nicolaus, I. Peeken, and H. Flores (2016), Sea ice algae
785 chlorophyll *a* concentrations derived from under-ice spectral radiation profiling platforms,
786 *Journal of Geophysical Research: Oceans*, doi:10.1002/2016JC011991.

- 787 Lange, B. A., H. Flores, C. Michel, J. F. Beckers, A. Bubnitz, J. A. Casey, G. Castellani,
788 I. Hatam, A. Reppchen, S. A. Rudolph, and C. Haas (2017), Pan-Arctic sea ice-algal chl *a*
789 biomass and suitable habitat are largely underestimated for multiyear ice, *Global Change*
790 *Biology*, pp. n/a–n/a, doi:10.1111/gcb.13742.
- 791 Lavoie, D., K. Denman, and C. Michel (2005), Modeling ice algal growth and decline in
792 a seasonally ice-covered region of the Arctic (Resolute Passage, Canadian Archipelago),
793 *Journal of Geophysical Research: Oceans*, *110*(C11), doi:10.1029/2005JC002922, c11009.
- 794 Laxon, S. W., K. A. Giles, A. L. Ridout, D. J. Wingham, R. Willatt, R. Cullen, R. Kwok,
795 A. Schweiger, J. Zhang, C. Haas, S. Hendricks, R. Krishfield, N. Kurtz, S. Farrell, and
796 M. Davidson (2013), CryoSat-2 estimates of Arctic sea ice thickness and volume, *Geophys.*
797 *Res. Lett.*, *40*, 732–737.
- 798 Leu, E., C. Mundy, P. Assmy, K. Campbell, T. Gabrielsen, M. Gosselin, T. Juul-
799 Pedersen, and R. Gradinger (2015), Arctic spring awakening – Steering principles be-
800 hind the phenology of vernal ice algal blooms, *Progress in Oceanography*, *139*, 151–170,
801 doi:10.1016/j.pocean.2015.07.012, overarching perspectives of contemporary and future
802 ecosystems in the Arctic Ocean.
- 803 Lizotte, M. P. (2001), the contributions of sea ice algae to antarctic marine primary pro-
804 duction , *American Zoologist*, *41*, 57–73.
- 805 Losch, M., D. Menemenlis, J. M. Campin, P. Heimbach, and C. Hill (2010), On the formu-
806 lation of sea-ice models: Part 1: Effects of different solver implementations and parame-
807 terizations, *Ocean Mod.*, *33*, 129–144, doi: 10.1016/j.ocemod.2009.12.008.
- 808 Marshall, J., A. J. Adcroft, C. N. Hill, L. Perelman, and C. Heisey (1997), A finite-volume,
809 incompressible Navier Stokes model for studies of the ocean on parallel computers, *J.*
810 *Geophys. Res.*, *102*(C3), 5753–5766, doi:10.1029/96JC02,775.
- 811 Meiners, K. M., M. Vancoppenolle, S. Thanassekos, G. S. Dieckmann, D. N. Thomas, J.-
812 L. Tison, K. R. Arrigo, D. L. Garrison, A. McMinn, D. Lannuzel, P. van der Merwe,
813 K. M. Swadling, W. O. Smith, I. Melnikov, and B. Raymond (2012), Chlorophyll *a* in
814 Antarctic sea ice from historical ice core data, *Geophysical Research Letters*, *39*(21), doi:
815 10.1029/2012GL053478, 121602.
- 816 Meiners, K. M., S. Arndt, S. Bestley, T. Krumpfen, R. Ricker, M. Milnes, K. New-
817 bery, U. Freier, S. Jarman, R. King, R. Proud, S. Kawaguchi, and B. Meyer (2017),
818 Antarctic pack ice algal distribution: Floe-scale spatial variability and predictabil-
819 ity from physical parameters, *Geophysical Research Letters*, *44*(14), 7382–7390, doi:

- 820 10.1002/2017GL074346, 2017GL074346.
- 821 Melbourne-Thomas, J., M. KM, M. CJ, C. Schallenberg, T. KL, and D. GS (2015), Algo-
822 rithms to estimate Antarctic sea ice algal biomass from under-ice irradiance spectra at
823 regional scales, *Marine Ecology Progress Series*, 536, 107–121, 10.3354/meps11396.
- 824 Melbourne-Thomas, J., M. KM, M. CJ, C. Schallenberg, T. KL, and D. GS (2016), Corri-
825 gendum: Algorithms to estimate Antarctic sea ice algal biomass from under-ice irradiance
826 spectra at regional scales, *Marine Ecology Progress Series*, 561, 261, 10.3354/meps11396.
- 827 Melnikov, I. A., E. G. Kolosova, H. E. Welch, and L. S. Zhitina (2002), Sea ice biological
828 communities and nutrient dynamics in the Canada Basin of the Arctic Ocean, *Deep Sea
829 Research Part I: Oceanographic Research Papers*, 49(9), 1623–1649, doi:10.1016/S0967-
830 0637(02)00042-0.
- 831 Michel, C., L. Legendre, S. Demers, and J.-C. Therriault (1988), Photoadaptation of sea-ice
832 microalgae in springtime: Photosynthesis and carboxylating enzymes, *Marine Ecology
833 Progress Series*, 50, 177–185.
- 834 Mock, T., and R. Gradinger (1999), Determination of Arctic ice algal production with a
835 new in situ incubation technique, *Marine Ecology Progress Series*, 177, 15–26.
- 836 Monod, J. (1949), The Growth of Bacterial Cultures, *Annual Review of Microbiology*, 3,
837 371–394, doi:10.1146/annurev.mi.03.100149.002103.
- 838 Mortensen, E., H. Hayashida, N. Steiner, A. Monahan, M. Blais, M. A. Gale, V. Galindo,
839 M. Gosselin, X. Hu, D. Lavoie, and C. J. Mundy (2017), A model-based analysis of
840 physical and biological controls on ice algal and pelagic primary production in Resolute
841 Passage, *Elem Sci Anth.*, 50(39).
- 842 Nicolaus, M., C. Katlein, J. A. Maslanik, and S. Hendricks (2012), Changes in Arctic sea
843 ice result in increasing light transmittance and absorption, *Geophys. Res. Lett.*, 39, 2699–
844 2700.
- 845 Perovich, D. K. (1996), The optical properties of sea ice, Ph.D. thesis.
- 846 Perovich, D. K., T. C. Grenfell, J. A. Richter-Menge, B. Light, W. B. Tucker III, and
847 H. Eicken (2003), Thin and thinner: Sea ice mass balance measurements during SHEBA,
848 *J. Geophys. Res.*, 108(C3)(8050).
- 849 Proshutinsky, A., M. Steele, J. Zhang, G. Holloway, N. Steiner, S. Häkkinen, D. M. Holland,
850 R. Gerdes, C. Köberle, M. Karcher, M. Johnson, W. Maslowsky, Y. Zhang, W. D. Hibler
851 III, and J. Wang (2001), The Arctic Ocean Model Intercomparison Project (AOMIP),
852 *EOS*, 82(51), 637–644.

- 853 Ricker, R., S. Hendricks, D. K. Perovich, V. Helm, and R. Gerdes (2015), Impact of
854 snow accumulation on CryoSat-2 range retrievals over Arctic sea ice: An observa-
855 tional approach with buoy data, *Geophysical Research Letters*, *42*(11), 4447–4455, doi:
856 10.1002/2015GL064081, 2015GL064081.
- 857 Ricker, R., S. Hendricks, F. Girard-Ardhuin, L. Kaleschke, C. Lique, X. Tian-Kunze,
858 M. Nicolaus, and T. Krumpfen (2017), Satellite-observed drop of Arctic sea ice
859 growth in winter 2015–2016, *Geophysical Research Letters*, *44*(7), 3236–3245, doi:
860 10.1002/2016GL072244, 2016GL072244.
- 861 Saenz, B. T., and K. R. Arrigo (2014), Annual primary production in Antarctic sea ice
862 during 2005–2006 from a sea ice state estimate, *Journal of Geophysical Research: Oceans*,
863 *119*, 3645–2678.
- 864 Saha, S., S. Moorthi, X. Wu, J. Wang, S. Nadiga, P. Tripp, D. Behringer, Y.-T. Hou, H.-y.
865 Chuang, M. Iredell, M. Ek, J. Meng, R. Yang, M. P. Mendez, H. van den Dool, Q. Zhang,
866 W. Wang, M. Chen, and E. Becker (2014), The NCEP Climate Forecast System Version
867 2, *Journal of Climate*, *27*(6), 2185–2208, doi:10.1175/JCLI-D-12-00823.1.
- 868 Sarthou, G., K. R. Timmermans, S. Blain, and P. Tréguer (2005), Growth physiology and
869 fate of diatoms in the ocean: a review, *Journal of Sea Research*, *53*(1–2), 25–42, doi:
870 10.1016/j.seares.2004.01.007, iron Resources and Oceanic Nutrients - Advancement of
871 Global Environmental Simulations.
- 872 Schünemann, H., and I. Werner (2005), Seasonal variations in distribution patterns
873 of sympagic meiofauna in Arctic pack ice, *Marine Biology*, *146*(6), 1091–1102, doi:
874 10.1007/s00227-004-1511-7.
- 875 Semtner, A. J. J. (1976), A model for the thermodynamic growth of sea ice in numerical
876 investigations of climate, *J. Phys. Oceanogr.*, *6*, 379–389.
- 877 Serreze, M. C., J. A. Maslanik, T. A. Scambos, F. Fetterer, J. Stroeve, K. Knowles,
878 C. Fowler, S. Drobot, R. G. Barry, and T. M. Haran (2003), A record minimum Arctic sea
879 ice extent and area in 2002, *Geophys. Res. Lett.*, *30*(1110)(3), doi:10.1029/2002GL016,406.
- 880 Serreze, M. C., M. M. Holland, and J. Stroeve (2007), Perspectives on the Arctic’s Shrinking
881 Sea-Ice Cover, *Science*, *315*(5818), 1533–1536, doi: 10.1126/science.1139,426.
- 882 Sibert, V., B. Zakardjian, F. Saucier, M. Gosselin, M. Starr, and S. Senneville (2010),
883 Spatial and temporal variability of ice algal production in a 3D ice–ocean model of the
884 Hudson Bay, Hudson Strait and Foxe Basin system, *Polar Research*, *29*(3), 353–378,
885 doi:10.1111/j.1751-8369.2010.00184.x.

- 886 Smith, R. E. H., M. Gosselin, and S. Taguchi (1997), The influence of major inorganic
887 nutrients on the growth and physiology of high Arctic ice algae, *J. Mar. Syst.*, *110*, 63–
888 70.
- 889 Søreide, J. E., M. L. Carroll, H. Hop, W. G. Ambrose Jr., E. N. Hegseth, and S. Falk-
890 Petersen (2013), Sympagic-pelagic-benthic coupling in Arctic and Atlantic waters around
891 Svalbard revealed by stable isotopic and fatty acid tracers, *Mar. Biol. Res.*
- 892 Steiner, N., M. Harder, and P. Lemke (1999), Sea-ice roughness and drag coefficients in
893 a dynamic-thermodynamic sea-ice model for the Arctic, *Tellus, A*, *51*, 964–978. doi:
894 10.1034/j.1600-0870.1999.00,029.x.
- 895 Stroeve, J., M. M. Holland, W. Meier, T. Scambos, and M. Serreze (2007), Arctic sea ice de-
896 cline: Faster than forecast, *Geophys. Res. Lett.*, *34*, L09501, doi:10.1029/2007GL029,703.
- 897 Stroeve, J. C., V. Kattsov, P. Barret, M. Serreze, T. Pavlova, M. Holland, and W. N. Meier
898 (2012a), Trends in Arctic sea ice extent from CMIP5, CMIP3 and observations, *Geophys.*
899 *Res. Lett.*, *39*, L16502, doi:10.1029/2012GL052,676.
- 900 Stroeve, J. C., M. C. Serreze, M. M. Holland, J. E. Kay, J. Maslanik, and A. P. Bar-
901 ret (2012b), The Arctic’s rapidly shrinking sea ice cover: a research synthesis, *Climatic*
902 *Change*, *110*(3-4), 1005–1027.
- 903 Sturm, M., J. Holmgren, and D. K. Perovich (2002), Winter snow cover on the sea ice of
904 the Arctic Ocean at the Surface Heat Budget of the Arctic Ocean (SHEBA), *J. Geophys.*
905 *Res.*, *107*(C10)(8047).
- 906 Tedesco, L., M. Vichi, J. Haapala, and T. Stipa (2010), A dynamic Biologically Active
907 Layer for numerical studies of the sea ice ecosystem, *Ocean Modelling*, *35*(1–2), 89–104,
908 doi:10.1016/j.ocemod.2010.06.008.
- 909 Tilling, R. L., A. Ridout, A. Shepherd, and D. J. Wingham (2015), Increased Arctic sea
910 ice volume after anomalously low melting in 2013, *Nature Geoscience*, *8*(8), 643–646,
911 doi:10.1038/ngeo2489.
- 912 Timco, G. W., and R. P. Burden (1997), An analysis of the shapes of sea ice ridges, *Cold*
913 *Reg. Sci. Technol.*, *25*, 65–77.
- 914 Tremblay, J.-É., K. Simpson, J. Martin, L. Miller, Y. Gratton, D. Barber, and N. M.
915 Price (2008), Vertical stability and the annual dynamics of nutrients and chlorophyll
916 fluorescence in the coastal, southeast Beaufort Sea, *Journal of Geophysical Research:*
917 *Oceans*, *113*(C7), n/a–n/a, doi:10.1029/2007JC004547, c07S90.

- 918 Vancoppenolle, M., and L. Tedesco (2017), Sea Ice Biogeochemistry: A Guide for Modellers,
919 in *Sea Ice*, edited by D. N. Thomas, WILEY Blackwell.
- 920 Vancoppenolle, M., R. Timmermann, S. F. Ackley, T. Fichefet, H. Goosse, P. Heil, K. C.
921 Leonard, J. Lieser, M. Nicolaus, T. Papakyriakou, and J.-L. Tison (2011), Assessment
922 of radiation forcing data sets for large-scale sea ice models in the Southern Ocean,
923 *Deep Sea Research Part II: Topical Studies in Oceanography*, 58(9–10), 1237–1249, doi:
924 10.1016/j.dsr2.2010.10.039, antarctic Sea Ice Research during the International Polar Year
925 2007-2009.
- 926 Vancoppenolle, M., K. M. Meiners, C. Michel, L. Bopp, F. Brabant, G. Carnat, B. Delille,
927 D. Lannuzel, G. Madec, S. Moreau, J.-L. Tison, and P. van der Merwe (2013), Role of sea
928 ice in global biogeochemical cycles: emerging views and challenges, *Quaternary Science*
929 *Reviews*, 79, 207–230, doi:10.1016/j.quascirev.2013.04.011, sea Ice in the Paleoclimate
930 System: the Challenge of Reconstructing Sea Ice from Proxies.
- 931 Wassmann, P., M. Reigstad, T. Haug, B. Rudels, M. L. Carroll, H. Hop, G. W. Gabrielsen,
932 S. Falk-Petersen, S. G. Denisenko, E. Arashkevich, D. Slagstad, and O. Pavlova (2006),
933 Food webs and carbon flux in the Barent Sea, *Progress in Oceanography*, 71(2-4), 232–287.
- 934 Webb, W. L., M. Newton, and D. Starr (1974), Carbon dioxide exchange of *Alnus rubra*,
935 *Oecologia*, 17(4), 281–291, doi:10.1007/BF00345747.
- 936 Welch, H. E., and M. A. Bergmann (1989), Seasonal development of ice algae and its
937 prediction from environmental factors near Resolute, N.W.T., Canada, *Can. J. Fish.*
938 *Aquat. Sci.*, 46, 1793–1804.
- 939 Werner, I., and R. Gradinger (2002), Under-ice amphipods in the Greenland Sea and Fram
940 Strait (Arctic): environmental controls and seasonal patterns below the pack ice, *Marine*
941 *Biology*, 140(2), 317–326, doi:10.1007/s00227-001-0709-1.
- 942 Zeebe, R. E., H. Eicken, D. H. Robinson, D. Wolf-Gladrow, and G. S. Dieckmann (1996),
943 Modeling the heating and melting of sea ice through light absorption by microalgae,
944 *Journal of Geophysical Research: Oceans*, 101(C1), 1163–1181, doi:10.1029/95JC02687.